Title
Hexane Cracking on ZSM-5 and Faujasite Zeolites: A QM/MM/QCT Study

Journal
Journal of Physical Chemistry C, 119(52)

ISSN
1932-7447

Authors
Tranca, DC
Zimmerman, PM
Gomes, J
et al.

Publication Date
2015-12-31

DOI
10.1021/acs.jpcc.5b07457

Peer reviewed

THE JOURNAL OF PHYSICAL CHEMISTRY C

Article

pubs.acs.org/JPCC

Hexane Cracking on ZSM-5 and Faujasite Zeolites: a QM/MM/QCT Study

D. C. Tranca,*[,†] P. M. Zimmerman,[‡,§] J. Gomes,[‡,§] D. Lambrecht,[‡,§] F. J. Keil,[†] M. Head-Gordon,[‡,§] and A. T. Bell[‡,§]

[†]Department of Chemical Engineering, Hamburg University of Technology, D-21073 Hamburg, Germany

[‡]Department of Chemical and Biomolecular Engineering, University of California, Berkeley, California 94720-1462, United States

[§]Department of Chemistry, University of California, Berkeley, California 94720-1461, United States

ABSTRACT: Quantum mechanics/molecular mechanics (QM/MM) models are applied to investigate the adsorption and cracking of *n*-hexane on ZSM-5 and Faujasite zeolite structures. These simulations account for the long-range electrostatic and midrange van-der-Waals interactions in the zeolite and provide energy barriers that are close to experimental data. The active acidic site was modeled by dispersion corrected density functional theory (DFT, ω B97X-D6-311/G*). The long-range interactions were calculated by molecular mechanics (MM). The adsorbed molecules under investigation are characterized by their thermodynamic properties (adsorption energy and enthalpy). The influence of the zeolite type on the thermodynamic properties is also pointed out. The results reveal that the kinetics of cracking is insensitive to differences in acid strengths. The thermodynamic data obtained are mainly influenced by the adsorption energy of *n*-hexane on ZSM-5 and/or Faujasite (Y) structures. The pore sizes of the zeolite types can lead to a stronger or weaker adsorption energy. Except for the thermodynamic property investigations in this article, the quasi-classical trajectory method (QCT) is used for investigating the pathways along metastable intermediates toward various cracking products. Not only the reaction barriers but also the reaction dynamics determine the reaction selectivity.

I. INTRODUCTION

Zeolitic materials are extensively employed in petroleum refining, petrochemicals production, and pollution control, to catalyze a variety of reactions such as alkylation, aromatization, and isomerization of hydrocarbons.[1−6] They exhibit both, Brønsted and Lewis acidic properties.[7] The active components of industrial cracking catalysts are made by hydrothermal treatment or steaming of Y zeolites.[8,9] Basic zeolites have generated interest because of their selectivity in catalysis and their adsorption properties.[7] In addition to increased hydrothermal stability, the steaming process leads to a dramatic increase of the cracking activity. Since cracking occurs at Brønsted acid sites, the observed activity enhancement is often attributed to the generation of the stronger Brønsted acid sites.

For understanding the details of catalytic alkane cracking reactions, quantum chemical calculations, in particular those based on density functional theory (DFT) combined with statistical thermodynamics and transition state theory have been employed successfully over the past few years.[10−16,19−27,84−86] In the literature, three different reaction mechanisms have been suggested: monomolecular,[28,29] bimolecular,[30−32] and oligomeric[32,33] reactions participate in cracking of hexane on the Brønsted acid sites of zeolites. These mechanisms have been distinguished on the basis of various transition states, relative reaction rates, observed product distribution, and deactivation behavior.

Frash and van Santen[16−18] reviewed quantum-chemical results of various elementary reactions in zeolites, like protolytic cracking of paraffins, protolytic dehydrogenation of paraffins, hydride transfer, skeletal isomerization, and alkylation. Reaction routes, transition state geometries and activation energies were considered. All results showed that the reaction proceeds via transition state with a nonclassical three-centered bond C(1)−C(2)−H(1) whereby the H(1) hydrogen is still bound to a zeolite oxygen. The geometry parameters of the TS and activation energies depend on the relative stability of the corresponding carbocations. Increasing the number of methyl groups attached to the carbenium centers leads to their stabilization which reduces the activation energies, and increases the distances from the carbenium centers to the zeolite oxygens. Variation of the cluster acid strength turned out to be a useful technique in quantum-chemical modeling of the acid zeolite catalyzed reactions.

Adsorption and cracking of *n*-alkane molecules on different zeolite structures such as ZSM-5,[8,9,34,35] FAU (Y),[8,9,34,35] and

Received: August 1, 2015
Revised: December 4, 2015
Published: December 4, 2015

DOI: 10.1021/acs.jpcc.5b07457
J. Phys. Chem. C 2015, 119, 28836−28853

MOR[8,9,34,35] have been experimentally investigated. In these studies, and many others, it has been shown that the differences in apparent activation energies can be entirely attributed to differences in heats of *n*-hexane adsorption. Extensive reviews of experimental results on hydrocarbon catalytic cracking in zeolites were published.[36−43]

An alkane molecule adsorbed in zeolites is first protonated, then a C−C bond cleavage occurs, resulting finally in alkanes and alkene fragments. Previous computational studies were directed toward identification of transition states (TSs) and activation energies for the different C−C bond cleavages.[16] This approach does not automatically result in the formation of multiple products formed from one given TS. Furthermore, identical products might form from different transition states. Alongside the pathway from the TS to the final products, several metastable intermediates may be created. The potential energy surfaces (PESs) are calculated for 0 K, and the TSs on the surfaces are first-order saddle points which, in general, will not coincide with free energy transition states.[46] Therefore, the standard approach for TS obtained for 0 K are not sufficient for finding product distributions. In previous investigations, Dellago et al.[44,45] and Bucko et al.[46] have used transition-path sampling (TPS) for investigating propane cracking on H−CHA. These authors could demonstrate that multiple reaction pathways from a given TS are possible owing to flat PESs in the zeolite. TPS uses predefined product basins while all other trajectories are discarded.

Additionally, Bucko et al.[46] investigated propane cracking using dispersion-corrected periodic DFT calculations in combination with ab initio molecular dynamics (AIMD) simulations, and free-energy integrations. The AIMD simulations showed that due to the weak specific interaction of the saturated molecule with Brønsted acid sites, the adsorption energy is considerably reduced at elevated temperature and that only a fraction of the molecules adsorbed within the zeolite is sufficiently close to the acid site to form a reactant complex for protonation. TPS showed that the preferred reaction mechanism is the protonation of a terminal methyl group. The direct proton attack on the C−C bond between the methyl and methylene groups occurs with a lower probability. Zimmerman et al.[85] calculated the product selectivity of pentane cracking in the H-MFI zeolite by dynamic first-principles QM/MM simulations. These simulations accounted for the electrostatic- and shape-selective interactions in the zeolite. Details of the reaction mechanism could be clarified. In particular a metastable intermediate could be detected where the proton is shared between two hydrocarbon fragments. The zeolite strongly stabilized these carbocations compared to the gas phase, and the conversion of this intermediate to more stable species determines the product selectivity.

In this article the QM/MM method as implemented in QCHEM program is used. The QM/MM method is combined with quasi-classical trajectory (QCT) calculations for studying the adsorption and cracking of *n*-hexane on ZSM-5 and Y zeolites. QCT is used to sample the dynamic degrees of freedom involved in the cracking of *n*-hexane on ZSM-5 and Y zeolites. Unlike TPS calculations, these simulations provide information on the distribution of products that are formed by reactions of *n*-hexane at Brønsted acid sites. Short-lived intermediate compounds are detected in this article.

QCT calculations identify the reaction pathways via which products are formed at a working reaction temperature of the catalyst and can thus give the distribution of products formed from the respective TS. Details are given below. Various QCT approaches have been employed previously. A review of classical trajectory calculations is presented by Porter,[64] various ab initio Molecular Dynamics approaches are described in the book by Marx and Hutter,[90] and Bolhuis et al.[45] exemplify transition path sampling. These authors also discuss many applications of the respective methods.

The kinetics of cracking and dehydrogenation of light alkanes has been calculated by several authors,[20−23,26,45,89] among others. In these articles different problems have been raised and solved such as, the reaction of hydrogen exchange and dehydrogenation of methane catalyzed by an acidic zeolite,[20] the product distributions for hexane cracking and also some experimental and theoretical kinetic data are presented in ref.[26] The idea of this article is to improve the theoretical models which exists, such that a resonable comparison between the experiments and theory can be done. Starting from a single TS we were able to find different products and all the intermediate states. This is an advantage over the existing methods, in which starting from a TS it was possible to find only one product.

The present paper has the following aims:

The adsorption and reaction pathways of hexane cracking in MFI and FAU zeolites at three realistic temperatures (673, 773, and 813 K) will be investigated by quasi-classical trajectory (QCT) calculations. Large cluster models (T276 and T400) will be employed in order to detect local minima and saddle points. Several hundred trajectories will be calculated. Dispersion corrections are included in the DFT calculations. This procedure samples the nonequilibrium reaction pathways after the TS which may be different from the potential energy paths.

The dynamics of the reactions will be calculated to obtain the evolvement of atomic and molecular distances as a function of time. This will reveal short-lived intermediates and the stabilization of intermediates.

The product distributions, rate constants, heats of adsorption will be calculated. In particular, the influence of the pore structures will be considered as the pore diameters between MFI and FAU are quite different. Temperature effects will be also considered.

The results will be compared with previous simulations of *n*-alkane cracking.

The organization of this paper is as follows. The theoretical description of the QM/MM approach, the QCT-MD method, calculation of rate constants and TSs used in this article and the way the thermodynamical data are calculated for $T > 0$ K are provided in section II. The results of the thermodynamic property calculations (e.g., adsorption energies, adsorption enthalpies and intrinsic adsorption energy and enthalpy) of *n*-hexane adsorbed on ZSM-5 and Y structures are presented in section III. In sections IV and V the trajectory calculations for different temperatures (673, 773, and 813 K) and the thermodynamic properties obtained for the products are described. Finally, the results are summarized.

II. COMPUTATIONAL DETAILS

A. QM/MM Calculations. The computations have been executed employing the QCHEM program.[47] Adsorption and cracking of *n*-hexane on ZSM-5 and Y (FAU) zeolite have been calculated by a QM/MM approach. The H-MFI and Y zeolites are represented by a T276 and a T400 cluster size, respectively, and the zeolite structures were taken from X-ray diffraction data.[48] For the ZSM-5 structure a Si atom was replaced by an

DOI: 10.1021/acs.jpcc.5b07457
J. Phys. Chem. C 2015, 119, 28836−28853

Al atom at the T12 site[49,50] and the resulting negative charge was compensated by a proton bonded to one of the neighboring framework oxygens. There is some evidence that the T12 position is favored.[49−51] Some calculations were executed for the T7 position (see Figure 1). As the Y zeolite is

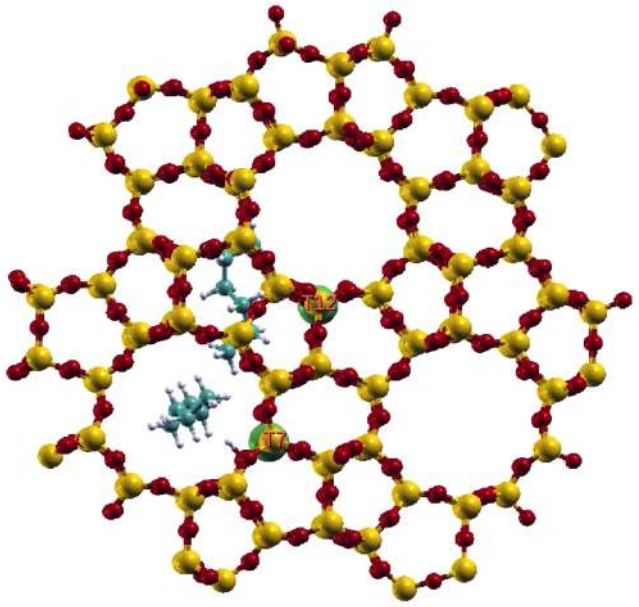

Figure 1. C_6H_{14} adsorbed on ZSM-5 zeolite. (Color codes: carbon - light blue, hydrogen -white, oxygen - light red, Silicon - light yellow, aluminum - light green.)

symmetric (cubic, Fd3m) it does not matter where the Al atoms are placed. The QM region is formed by a T5 cluster centered on the acid site and the adsorbed molecules, whereas other atoms are modeled by MM simulations.

The present QM/MM implementation follows an electrostatic embedding scheme originally developed by Field et al.[52] and Lyne et al.[53] This approach was then implemented into QCHEM by Woodcock et al.[54] and Zimmerman et al.[55] In the present QM/MM approach the QM region is polarized by the MM region using point charges derived from QM to accurately represent the lattice electrostatic potential. An overview over various QM/MM schemes is presented by Lin and Truhlar.[56] To divide the QM and MM regions smoothly, a single hydrogen link atom is used to replace a Si−O bond at the terminus of the QM cluster. The terminating H atoms were placed along each of the terminal Si−O bonds at a distance of 0.92 Å from the terminal Si atom. To achieve charge neutrality of the MM subsystem, a fraction of the link atom charge was added to its covalently bonded neighbor and the charge on the link atom was set to zero.[55] The MM region was described by a force field of CHARMM[57] type. Selection of charge and Lennard-Jones(6,12) parameters for Si and O was done by reducing the error between QM/MM and QM calculations.[55] The following values were taken from ref 55: ϵ_{Si} = 0.2 kcal/mol, ϵ_O = 0.075 kcal/mol, R_{Si} = 2.2 Å, and R_O = 1.77 Å for the framework atoms. Lennard-Jones parameters for hydrocarbons were taken from CHARMM.[57] The atoms in the QM part were fully relaxed, while the MM part was kept in its crystallographic positions.

The system geometries of the QM part and QCT-MD simulations were carried out employing the B97 6-31G* basis set completed by dispersion corrections according to Grimme.[51,58] For the reactant systems, additional one step energy calculations were executed employing dispersion corrected range-separated ω B97X-D 6-311G**/ω B97X-D 6-311++G(3df,3pd)/B97 6-31G* basis set,[81,82] to obtain high quality thermodynamics properties. Transition state (TS) energy calculations were executed employing the dispersion corrected range-separated ω B97X-D 6-311G** basis set.[81,82] This basis set was observed to give very good results compared to experimental data. Vibrational frequency computations were performed on all intermediates and transition states. Whether local minima or TSs were obtained, respectively, has been checked by eigenvalue analysis.[59,60]

B. Transition States, Rate Constants, Quasiclassical Trajectory Molecular Dynamics (QCT-MD) Calculations. The transition states were calculated by the partitioned rational function optimization (P-RFO) algorithm[61] as implemented in QCHEM. For this purpose the chemical bond, whose cleavage by the adjacent acid site is intended, is initially positioned in resonable distances to the active site. Whether the transition states have been found by P-RFO was checked by means of vibrational frequencies (one imaginary frequency should be there). This procedure was repeated for all three possible bonds (C_1−C_2, C_2−C_3, and C_3−C_4, where C stands for carbon) to be broken.

To follow the trajectories of the products downhill the PES quasiclassical trajectory molecular dynamics (QCT-MD) calculations were executed as implemented in QCHEM and described by Lambrecht et al.[62] This procedure is known variously as "ab initio molecular dynamics" (AIMD) or "Born−Oppenheimer molecular dynamics" (BOMD). The quasiclassical trajectories are obtained by propagating the classical equations of motion, while the required potential gradients (forces) and energies are computed quantum mechanically. Early developments of this approach are presented in refs 63−65. An up-to-date review of ab initio MD approaches is given in a book by Marx and Hutter.[90] QCT-MD puts vibrational energy into each mode in the initial velocity setup step. The present approach[62] describes vibrations by the harmonic approximation

$$E^n_{vib}(n) = h\nu_m\left(n + \frac{1}{2}\right) \tag{1}$$

and the modes are uncoupled such that the assigment can be performed for all modes independently (normal modes). The subscript m denotes the normal mode m, and n is the quantum number. The probability p^m_n that the mth mode is in the state n is determined from the Boltzmann factor

$$p^m_n = \frac{1}{Z_m}\exp(-E^n_{vib}(n)/kT) = \frac{1}{Z_m}\exp(-\Theta_m(n + 1/2)/T) \tag{2}$$

where Θ_m is the vibrational temperature of the mode, and Z_m is the vibrational partition function $Z_m = \sum_n \exp(-E^n_{vib}(n)/((kT))$. The energy levels n are found according to

$$n = -\left[\frac{T}{\Theta_m}(\ln p^m_n + \ln Z_m) - \frac{1}{2}\right] \tag{3}$$

DOI: 10.1021/acs.jpcc.5b07457
J. Phys. Chem. C 2015, 119, 28836−28853

where p is a random number $p \in [0,1]$ and $\lceil\rceil$ is the ceiling function. This assignment distributes the initial vibrational levels according to Boltzmann statistics at temperature T. The initial velocities along mode m are given by

$$q_m^{(0)} = \pm\sqrt{\frac{2E_{\mathrm{vib}}^m(n) - V(q_m^{(0)})}{\mu_m}} \tag{4}$$

where V is the potential energy and μ_m the reduced mass. These velocities are consistent with QM populations of each harmonic vibrational mode based on the canonical ensemble at the TS structure (673, 773, and 813 K). The QCT approach assures that the initial nuclear velocities are selected as to represent the quantum effects of nuclear motion. Each mode contains at least the zero-point energy (ZPE). The initial geometries have to be confined to within the classical turning points to obtain real-valued velocities. The signs of the initial velocities are chosen at random, and the normal mode velocities are transformed into Cartesian velocities. The movement starts from the transition state in the direction of products or reactants, respectively. To this end, the transition state mode was populated in the product or reactant direction. A more complete sampling approach would be an initiation of trajectories with randomized displacements along vibrational modes.[83] Limitations(zero-point leak (ZPL)) of the QCT-MD owing to classical description of the trajectories are elucidated by Czako et al.,[66] among others. For the MD calculations 2000 time steps of 0.48 fs each were taken. To check the effect of the number of time steps, some examples up to 4000 time steps were executed. Fifty trajectories for each transition state and each of the temperatures (673, 773, and 813 K) were calculated. QCT simulations that begin from a TS identify the pathways via which products are formed at a given reaction temperatures. Therefore, by means of QCT one can obtain the product distribution formed from the chosen TS.

Additionally, intrinsic reaction coordinate (IRC) steepest descend path calculations starting from a TS down to products on a PES were executed.

C. Finite Temperature Corrections and Intrinsic Rate Coefficients. Adsorption energies at T = 0 K were calculated as

$$\Delta E_{\mathrm{ads}}^{T=0} = E_{\mathrm{complex}} - (E_{\mathrm{alkane}} + E_{\mathrm{ZSM-5}}) \tag{5}$$

where E_{complex} is the total electronic energy of the adsorption complex, E_{alkane} is the total electronic energy of the alkane of optimized structure in vacuum, and $E_{\mathrm{ZSM-5}}$ is the total energy of the clean zeolite. Zero point corrected vibrational adsorption energies, $\Delta E_{\mathrm{ads,0}}^{T=0}$, were obtained from

$$\Delta E_{\mathrm{ads,0}}^{T=0} = \Delta E_{\mathrm{ads}}^{T=0} + \sum_{ip}^{\mathrm{modes}} \frac{1}{2}h\omega_{ip} - \sum_{is}^{\mathrm{modes}} \frac{1}{2}h\omega_{is} - \sum_{iA}^{\mathrm{modes}} \frac{1}{2}h\omega_{iA} \tag{6}$$

where $\sum_{\mathrm{ip}}^{\mathrm{modes}} \frac{1}{2}h\omega_{\mathrm{ip}}$ are the vibrational frequencies corresponding to the adsorbed system, $\sum_{\mathrm{is}}^{\mathrm{modes}} \frac{1}{2}h\omega_{\mathrm{is}}$ are the vibrational frequencies corresponding to the ZSM-5 or FAU surface and $\sum_{\mathrm{iA}}^{\mathrm{modes}} \frac{1}{2}h\omega_{\mathrm{iA}}$ are the vibrational frequencies corresponding to the gas phase molecule.

For molecules in the gas phase the rigid-rotator harmonic oscillator approximation[67] was used for calculating the finite temperature correction to the adsorption enthalpy. For all adsorbate and transition state complexes, corrections for finite temperatures were calculated assuming immobile adsorption, that is, complete conversion of frustrated rotational and translational degrees of freedom into vibrations. As far as enthalpies are concerned this approximation is justified because their sensitivity to variations in the harmonic frequency values is weak.[68,69] For the calculation of adsorption entropies this treatment usually overestimates the entropy loss during adsorption.[68−70] The intrinsic rate coefficients were calculated from conventional transition state theory[71−73]

$$k(T) = \frac{kT}{h}\frac{Q_{\mathrm{TS}}(T)}{Q_{\mathrm{R}}(T)}\exp^{[-E^{\ddagger}/\mathrm{RT}]} \tag{7}$$

where k is the Boltzmann constant, h is the Planck constant, T is the absolute temperature, and $E^{\ddagger}$ is the difference in electronic energies betwen the transition state and reactant state. The term R represents the gas constant. With Q_{TS} and Q_{R}, we denote the partition functions of the transition state and the reactant state, respectively, evaluated using only vibrational modes.

III. THERMODYNAMIC PROPERTIES AND TRANSITION STATES

A. Hexane Adsorbed on ZSM-5 and Y Zeolite. In this section the results of the adsorption calculations for C_6H_{14} adsorbed on the T12 site of ZSM-5 (−88 kJ/mol) and Y zeolite surface are presented, see Table 1 and Figure 1 and 2. Similar calculations have been done for *n*-hexane cracking on ZSM-5 at T7 site which resulted in an adsorption energy of E_{ads} = −79 kJ/mol. The difference between T12 and T7 site is only 9 kJ/mol. Different acid sites for ZSM-5 structure only weakly influence the adsorption energies and thermodynamical properties of the system.

Table 1. Adsorption Energies for C_6H_{14} on ZSM and Y Zeolites and also Adsorption Enthalpies for Reactant Molecules at $T > 0$ K[a]

C_6H_{14}	$\Delta E_{\mathrm{ads}}^{0\mathrm{K}}$ [kJ/mol]	T [K]	ΔH_{ads} [kJ/mol]	ΔH_{exp} [kJ/mol]
ZSM5	−88	423	−86	
		773	−81	−80 ± 6
FAU	−37	423	−30	−38, − 50 ± 3
		773	−25	-

[a]Experimental data from Babitz et al.[8,9] The value of −38 kJ/mol[74] for adsorption enthalpy corresponds to a Si/Al ratio of 6.4 and the value of −50 ± 3[8,9] kJ/mol corresponds to a Si/Al of 6.1. All values are in kJ/mol.

The higher adsorption energy for hexane adsorbed on ZSM-5 compared to the Y zeolite is due to the smaller pore size of ZSM-5 relative to Y zeolite which has large cages so that a lot of space is left between the zeolite framework and the adsorbate.

The experimental values[8,9] of the adsorption enthalpies fit very well to our theoretical data.

For the adsorption enthalpies of C_6H_{14} on Y zeolite, the experimental values are around −38 kJ/mol[74] for T = 423 K and a Si/Al ratio of 6.4, and −50 ± 3 kJ/mol[8,9] for a Si/Al ratio of 6.1. The value of the theoretical adsorption enthalpy of −30 kJ/mol at 423 K is close to the experimental data of

DOI: 10.1021/acs.jpcc.5b07457
J. Phys. Chem. C 2015, 119, 28836−28853

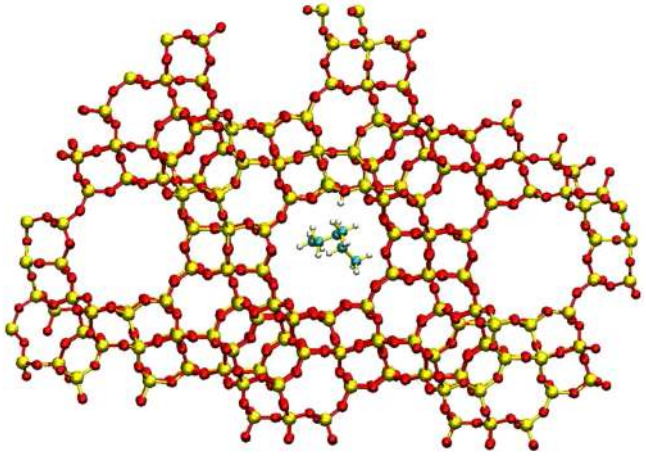

Figure 2. C_6H_{14} adsorbed on Y zeolite. (Color codes: carbon - light blue, hydrogen - white, oxygen - light red, silicon - light yellow, aluminum - light green).

−38 kJ/mol. The difference of 8 kJ/mol between theory and experiment may be partly accounted for by the difference in the Si/Al ratio. The adsorption energy and enthalpy values obtained for *n*-hexane molecule adsorbed on Y structure show that the *n*-hexane molecule is weaker adsorbed on Y compared to ZSM-5.

B. Transition State Geometries. Transition state calculations (TS) have been performed for cracking reactions of hexane on ZSM-5 and Y zeolite surfaces using the QM/MM method as implemented in QCHEM program[47] (see Figure 3). Three different types of TS for ZSM-5 and Y zeolites have been calculated:

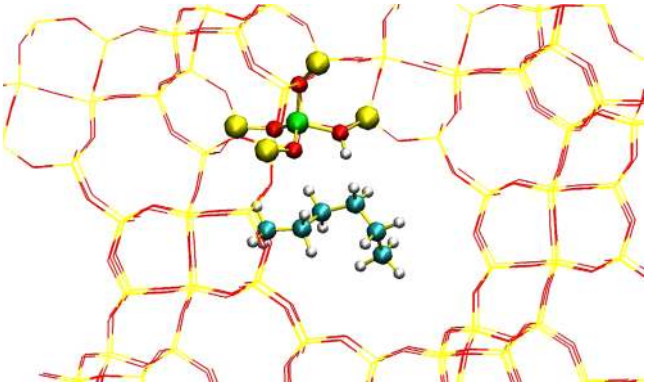

Figure 3. QM/MM region for the Y zeolite. The T5 QM region centered on the Al site is highlighted. The center Al site is shown with spheres. (Color codes: carbon - light blue, hydrogen - white, oxygen - light red, silicon - light yellow, aluminum - light green.)

- the TS between C_1-C_2 atoms of C_6 H_{14}
- the TS between C_2-C_3 atoms
- the TS between C_3-C_4 atoms

The TS geometries for monomolecular cracking of C_6 H_{14} on ZSM-5 and Y are shown in Figure 4. This figure shows the penta-coordinated alkanium ion forming the transition state. The interatomic distances are $d(O_4..H_3)$= 1.79 Å, $d(H_3..C_2)$ = 1.23 Å, and $d(C_1..C_2)$ = 1.8 Å for ZSM-5 surface, while for the Y zeolite we have found $d(O_4..H_3)$ = 1.68 Å, $d(H_3..C_2)$ = 1.32 Å, and $d(C_1..C_2)$ = 1.74 Å, respectively.

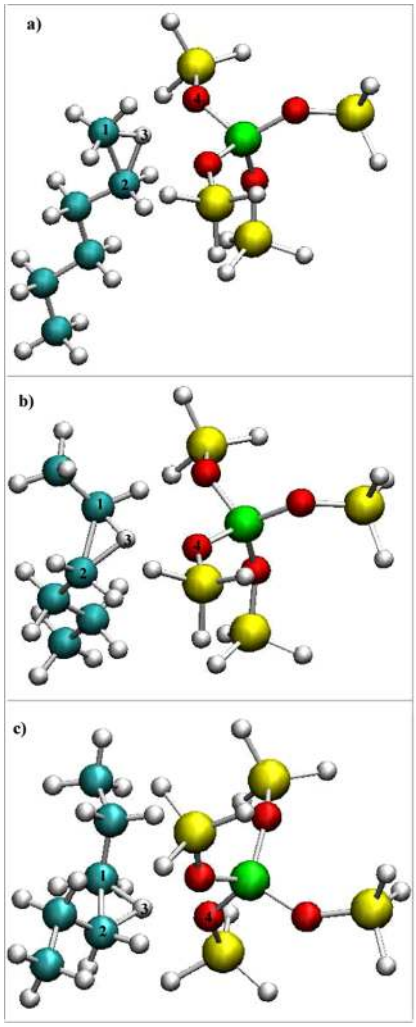

Figure 4. Transition state for cracking of C_6H_{14} on ZSM-5 and Y: (a) TS structure for cracking between the C_1-C_2 carbons; (b) TS structure for cracking between the C_2-C_3 carbons; (c) TS structure for cracking between the C_3-C_4 carbons. The distances (i) for ZSM-5 are the following $d(C_1...C_2)$ = 1.8 Å, $d(H_3...C_2)$ = 1.23 Å, $d(O_4...H_3)$ = 1.79 Å; (ii) for Faujasite are the following $d(C_1...C_2)$ = 1.74 Å, $d(H_3...C_2)$ = 1.32 Å, $d(O_4...H_3)$ = 1.68 Å. (Color codes: carbon - light blue, hydrogen - white, oxygen - light red, silicon - light yellow, aluminum - light green.)

The shorter distance between the oxygen belonging to the Y-zeolite structure and the proton compared to the ZSM-5 reveals that the TS for ZSM-5 is attracted by the opposite pore wall more strongly because of the shorter distance to that wall. The shorter distance between the oxygen and the proton for the Y zeolite leads to a faster cracking reaction (see Table 3) and consecutively the proton is transferred faster back to the zeolite lattice. All these processes play an important role in the formation of the final products (see Tables 4−7) .

C. Transition State Thermodynamic Properties. The intrinsic activation energies for cracking reactions on ZSM-5 are very close together for all three TSs and give values between 168−185 kJ/mol (see Table 2) . The differences between them are 2−17 kJ/mol and these differences are due to distinct TS configurations. The size of the chain and the dynamics which take place inside *n*-hexane at high temperatures make the system to behave different when it is cracked at different positions. Similar activation energies have been obtained for the

DOI: 10.1021/acs.jpcc.5b07457
J. Phys. Chem. C 2015, 119, 28836−28853

Table 2. Results for Intrinsic Activation Energies of C_6H_{14} on ZSM-5 and Y Zeolites in kcal/mol[a]

C_6H_{14}	$E_{activation}$ [kJ/mol]	$E^{(1)-(4)}_{activation}$ [kJ/mol]
C_1-C_2 (ZSM-5)	185	
C_2-C_3 (ZSM-5)	183	190(1)
C_3-C_4 (ZSM-5)	168	154(2), 149(3)
C_1-C_2 (FAU)	168	
C_2-C_3 (FAU)	147	138−176(4)
C_3-C_4 (FAU)	133	

[a]The value for reference (1) was taken from Tranca et al.,[84] reference (2) was taken from Maihom et al.,[75] reference (3) was taken from Babitz et al.[8] and from Bokhoven et al.,[87] and the values for reference (4) were taken from Babitz et al.[8,9]

bond cracking between C_1-C_2 and C_2-C_3 on ZSM5 zeolite (Table 2) . Breaking between the C_3-C_4 bond it is much easier (168 kJ/mol), as can be observed from the results of the activation energy. The entropy of the cracked molecule fractions is larger for C_3-C_4 than for C_1-C_2 cleavage (see Table 3). The C_3-C_4 cracking will lead to the formation of propane and propene molecules which are the main products of *n*-hexane cracking. That the center bonds show a lower activation energy has been observed earlier; see, for example, refs 16 and 26. These authors attribute this finding to the greater stability of the carbonium ion formed.

The ω B97X-D/6-31G* basis set used in this article is in good accord with other basis sets such as MO6−2X[75] for which the intrinsic activation energy is 154 kJ/mol for C_3-C_4 cracking. From the experimental data[8,87] we have a value of 149 kJ/mol. For the TS C_2-C_3, other theoretical results using full DFT calculations have reported a value of 190 kJ/mol[84] for the intrinsic activation energy. This activation energy is very close to the value we have reported in this article to be 183 kJ/mol using QM/MM method.

Also for the Y simulations, the theoretical intrinsic activation energies are in accordance with the experimental data,[8,9] which have been reported to be between 138−176 kJ/mol.[8,9] From the intrinsic activation energy calculations one notices that different zeolite structures certainly influence the intrinsic thermodynamic properties of the systems.

Table 3 summarizes intrinsic activation enthalpies and reaction rate constants for all studied reactions. All finite temperature corrections are based on unscaled harmonic normal modes obtained by diagonalization of the full dynamical matrices of the reactant and transition states. The intrinsic activation enthalpy for ZSM-5 lies between 152−182 kJ/mol and the experimental intrinsic activation enthalpy is around 191 kJ/mol[77] for T = 773 K. The value of 152 kJ/mol for the intrinsic activation energy for TS C_3-C_4 is in good agreement with other publications[55] in which the QCHEM method has been used for *n*-hexane adsorbed on ZSM-5 and for which the intrinsic activation enthalpy is 152 kJ/mol.[55] The experimental value is averaged over all TSs, while our computational data are for each TS between C_1-C_2, C_2-C_3, or C_3-C_4 separately. The theoretical value of 152 kJ/mol for C_6H_{14} (C_3-C_4) is obtained when the C−C bond is protonated, while the values of 182 and 179 kJ/mol for the structures C_6H_{14} (C_1-C_2) and C_6H_{14} (C_2-C_3), respectively, are obtained when the H−O bond is protonated. The experimental value of 191 kJ/mol is in good accordance with all calculated values.

The difference in activation enthalpies between the two zeolite structures is around 16−50 kJ/mol which corresponds to the differences in the adsorption energies and is therefore related to the pore structure of the two zeolites.[76,78-80]

The calculated activation entropies are always negative. The activation entropy deals with how the energy within the molecule must be redistributed for the reaction to occur. The negative values for $\Delta S^{\ddagger}_{int}$, which always occur for bimolecular reactions, indicate that entropy decreases upon achieving the transition state, because the activated complex is more "ordered" than the free molecule. For the C_1-C_2 TS the adsorption enthalpy is 30 kJ/mol lower than for the C_3-C_4 TS. The entropy changes the opposite way from −15 to −17 J/mol/K. This could be interpreted as an example of the compensation effect.

As can be seen from Table 3, the intrinsic rate constants for various cracking reactions are different by orders of magnitude for both zeolites, but the differences are larger for ZSM-5. As can be observed from Table 3, a stronger adsorption means that a higher adsorption enthalpy leads to a lower intrinsic rate constant.

IV. QUASICLASSICAL TRAJECTORIES (QCT-MD) CALCULATIONS

A. Static Description of *n*-Hexane Cracking in H-MFI and FAU. Once the TS is known, there are different approches to follow the reaction path. The IRC calculation starts from the TS and then follows the minimum energy path (MEP) to

Table 3. Intrinsic Activation Enthalpy ($\Delta H^{\ddagger}_{int}$), Intrinsic Activation Entropy ($\Delta S^{\ddagger}_{int}$), Activation Free Energy ($\Delta G^{\ddagger}_{int}$ [kJ/mol]), and Rate Constant (k_{int}) for Cracking of C_6H_{14} on ZSM-5 and Y[a]

C_6H_{14}	T [K]	$\Delta H^{\ddagger}_{int}$ [kJ/mol]	$\Delta H^{\ddagger}_{int}$(exp) [kJ/mol]	$\Delta S^{\ddagger}_{int}$ [J/mol/K]	$\Delta G^{\ddagger}_{int}$ [kJ/mol]	k_{int} [1/s]
C_1-C_2 (ZSM-5)	573	183		−14	191	0.48×10^{-4}
	773	182	191	−15	194	$0.13 \times 10^{+1}$
C_2-C_3 (ZSM-5)	573	180		−15	189	0.70×10^{-4}
	773	179	191	−17	192	$0.16 \times 10^{+1}$
C_3-C_4 (ZSM-5)	573	153		−16	162	0.19×10^{-1}
	773	152		−17	166	$0.10 \times 10^{+3}$
C_1-C_2 (FAU)	573	166		−13	174	0.17×10^{-2}
	773	165		−14	176	$0.19 \times 10^{+2}$
C_2-C_3 (FAU)	573	145		−13	152	$0.16 \times 10^{+0}$
	773	143		−15	155	$0.56 \times 10^{+3}$
C_3-C_4 (FAU)	573	132		−12	138	$0.28 \times 10^{+1}$
	773	131		−13	141	$0.48 \times 10^{+4}$

[a]Experimental data ($\Delta H^{\ddagger}_{int}$(exp)) from ref 77. The value of 151.8 for the intrinsic activation enthalpy was taken from ref 55.

DOI: 10.1021/acs.jpcc.5b07457
J. Phys. Chem. C 2015, 119, 28836−28853

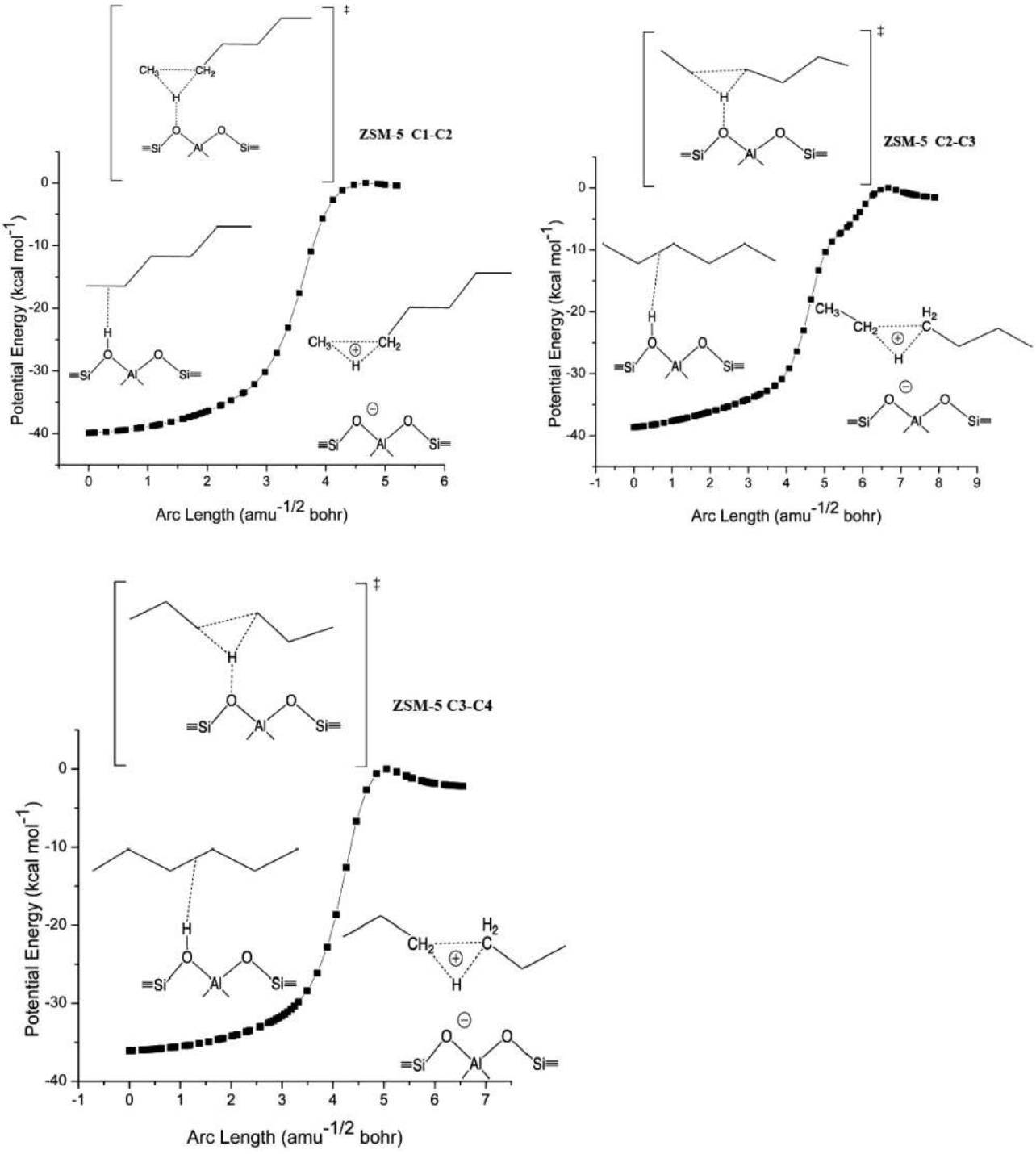

Figure 5. IRC pathways for cracking TS C_1-C_2 (top, left), TS C_2-C_3 (top, right), and TS C_3-C_4 (bottom) on ZSM-5. All IRC paths arrive in the reverse direction with C_6 coordinated to the acid site, while forward direction IRC paths end at C−H−C quasistable intermediates.

reactants and subsequently toward the products. The calculation is valuable for verifying that the TS found connects the reactants to the corresponding products. The IRC calculations have been done using the QCHEM program. For the reactants it was found that *n*-hexane adsorbed on the Brønsted acid side of ZSM-5 or FAU. On the product side the IRC simulations ended at a C−H−C intermediate state; see Figures 5 and 6. The structures of the C−H−C intermediates are shown in Figures 8i and 9e for TS C_2-C_3 and C_3-C_4 for ZSM-5 and in Figures 12b and 13b for FAU.

In anticipation of the dynamics simulations, it should be mentioned that these C−H−C intermediates are important states in the formation of further products and/or reactant states (Figures 8i and 9e and Figures 12b and 13b). Starting from a C−H−C state the adsorbed molecule can form different types of products such as $C_3H_8 + C_3H_6$, $C_2H_4 + C_4H_{10}$, and $C_2H_6 + C_4H_8$ or can lead to the formation of different intermediate states such as alkoxides, alkanes, and alkenes.

All these structures formed depend in general on the temperature at which the system is cracked. For a lower temperature value (T = 673 K) much more intermediate

DOI: 10.1021/acs.jpcc.5b07457
J. Phys. Chem. C 2015, 119, 28836−28853

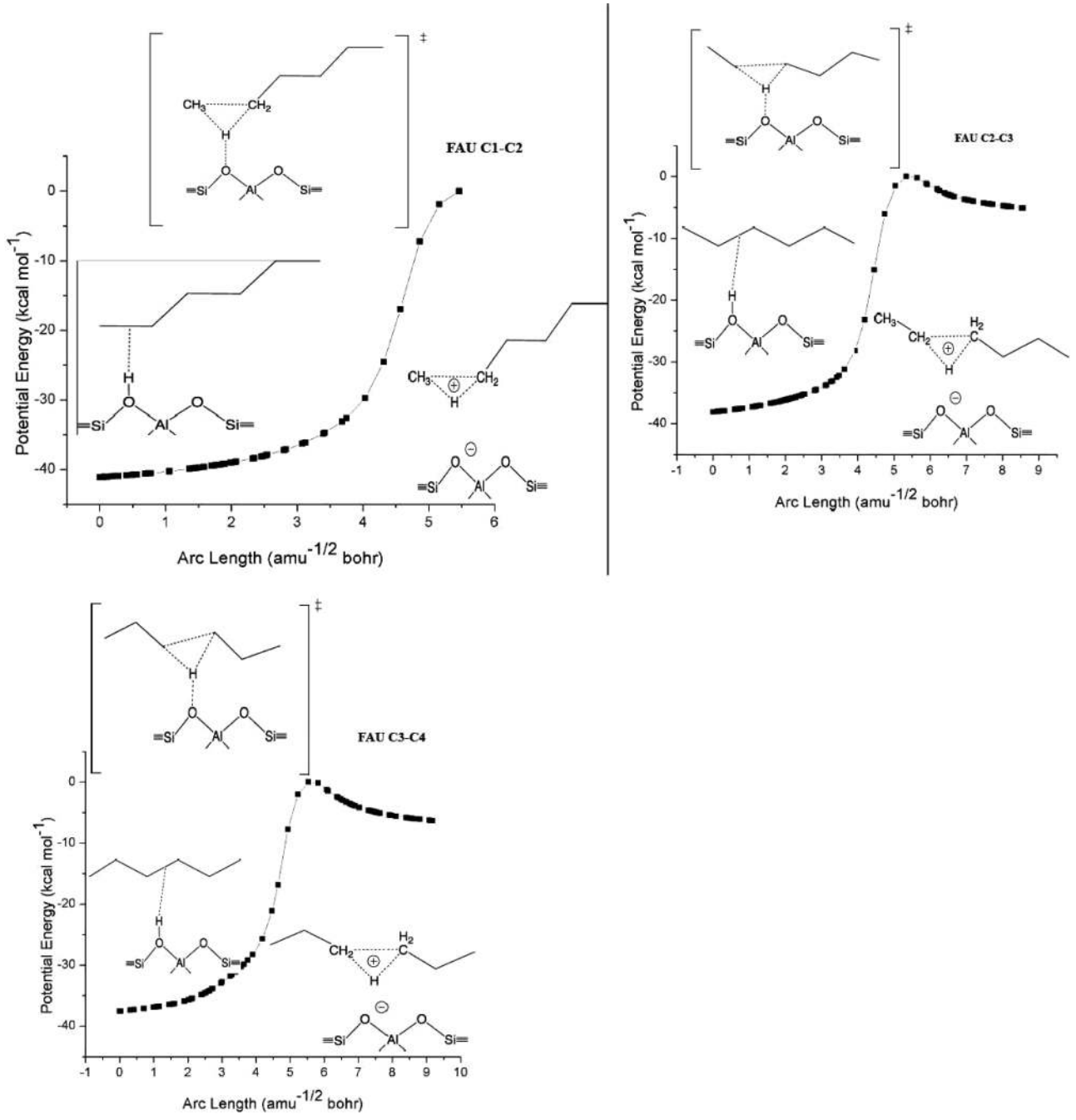

Figure 6. IRC pathways for cracking TS C_1-C_2 (top, left), TS C_2-C_3 (top, right), TS C_3-C_4 (bottom) on FAU. All IRC paths arrive in the reverse direction with C_6 coordinated to the acid site, while forward direction IRC paths end at C−H−C quasi-stable intermediates.

structures are obtained and less final products are formed, as expected. When the temperature is increasing (T = 813 K) more final products and less intermediate structures are obtained. Many of the reaction pathways leading from the metastable intermediate to final products were found by analyzing the path of the cracking system (Figures 12 and 13).

The reaction pathways shown in Figures 12 and 13 suggest that reactants passing through TS C_2-C_3 and TS C_3-C_4 will form a metastable C−H−C intermediate, which will react to form C_2 and C_3 alkanes, alkoxide, and alkenes.

B. Trajectories of C_6H_{14} on ZSM-5. In this section, results of QCT (Quantum-Classical) trajectories of C_6H_{14} cracking on ZSM-5 are presented. Trajectories are initiated at TS C_1-C_2, TS C_2-C_3, and TS C_3-C_4 and are run for 1 ps. At the end of the reaction path when molecules settle into quasistable structures, vibrational motions can be observed resulting from potential energy transfer into kinetic energy as the reaction proceeds downhill from the TS. Trajectory simulations have been executed for three different temperatures 673, 773, and 813 K. The products obtained have been compared with experimental data. For three temperatures, 50 trajectories have been simulated starting from each of the TS, that means 450 trajectories each for ZSM-5 and FAU.

For C_1-C_2 cracking fewer trajectories (approximately 20) have been calculated because only methane and pentene were always observed as stable products. The products and the intermediate states obtained are shown in Figure 7. The cracking at the C_1-C_2 leads to two major products groups

DOI: 10.1021/acs.jpcc.5b07457
J. Phys. Chem. C 2015, 119, 28836−28853

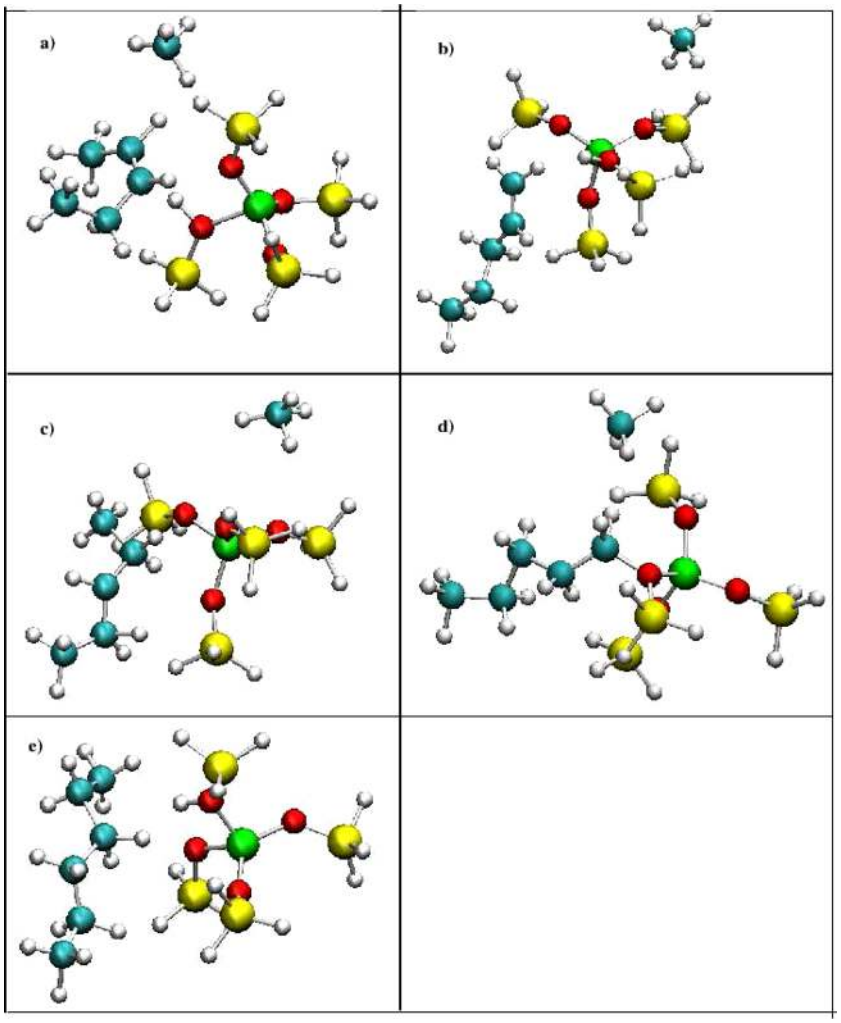

Figure 7. Structure calculations for C_6H_{14} C_1-C_2 on ZSM-5 after 1 ps: (a) CH_4 + *cis*-2-pentene; (b) CH_4 + 1-pentene; (c) CH_4 + C_5H_{11}; (d) alkoxide for CH_4 + $C_5H_{11}O$; (e) recrosing. (Color codes: carbon - light blue, hydrogen - white, oxygen - light red, silicon - light yellow, aluminum - light green.)

CH_4 + *cis*-2-pentene and CH_4 + 1-pentene. The products presented in Figure 7 are the results of the trajectory calculations. Details of the chronological and spatial sequence of the reaction steps will be explained for the C_2-C_3 and C_3-C_4 cracking below. QCT simulations show the full spectrum of the products that form from a TS.

In Table 4 and Figures 8a–i the QCT structures, after 1 ps, of the C_6H_{14} C_2-C_3 on ZSM-5 are shown. The QCT trajectory runs give distributions of products and intermediates. The major products that were formed within 1 ps were (a) C_2H_6 + 1-butene; (b) C_2H_6 + *cis*-2-butene; and (c) C_2H_4 + C_4H_{10}, and the intermediate products which have been obtained for this structure are (a) C_2H_5 + C_4H_{10}; (b) alkoxide (C_2H_5O + C_4H_{10}); (c) alkoxide (C_4H_9O + C_2H_6); and (d) C_2H_6 + C_4H_9. The percentage of intermediates formed decreases, and more final product trajectories are obtained when increasing the temperature from 673 to 813 K. The intermediate structure C_2H_6 + C_4H_9 decreases from 16% at 673 K to 8% at 813 K. In the same manner, the intermediate structure C_2H_5 + C_4H_{10} decreases from 4% at 673 K to 2% at 813 K and the alkoxide intermediate structure decreases from 20% at 673 K to 16% at 813 K, whereas, the amount of final products increases, e.g., C_2H_6 + 1-butene increase from 4% at 673 K to 14% at 813 K and C_2H_4 + C_4H_{10} goes from 2% to 6% at 813 K. From Table 4 it can be seen that between 28% and 38% of the QCT trajectories are, even after 1 ps, in the C–H–C bond streching and between 12% and 18% of QCT trajectories are recrossing into the reactant structures.

In Table 5 and Figure 9 QCT trajectories of C_6H_{14} C_3-C_4 on ZSM-5 are shown. Here as final products were obtained: (a) C_3H_8 + C_3H_6 and (b) C_3H_8 + cyclopropane. The cyclopropane molecule is a stable structure. The molecule can stay in this structure for a very long time or it could open via a diradical followed by a rearrangement of hydrogen atoms to form propene. An adsorption energy of 167.7 kJ/mol has been found for both products C_3H_8 + C_3H_6 and C_3H_8 + cyclopropane. One observes from the adsorption energies that propene plus propane has the same stability as propane and cyclopropane. Similar conclusions are also avaible for Y zeolite. The molecules C_3H_8 + C_3H_7 and alkoxides were observed as intermediate structures. The temperature effects on this system are very small. A small decrease of the alkoxide intermediates from 12% at 673 K to 10% at 813 K can be observed (Table 4). The number of bond streching trajectories is approximately 12% at 813 K and the number of QCT trajectories which are recrossing for forming the reactants goes up to 30% at 813 K.

For TS C_2-C_3 structure an additional calculation for 4000 time steps (2 ps) was executed. This structure after 2000 steps

DOI: 10.1021/acs.jpcc.5b07457
J. Phys. Chem. C 2015, 119, 28836–28853

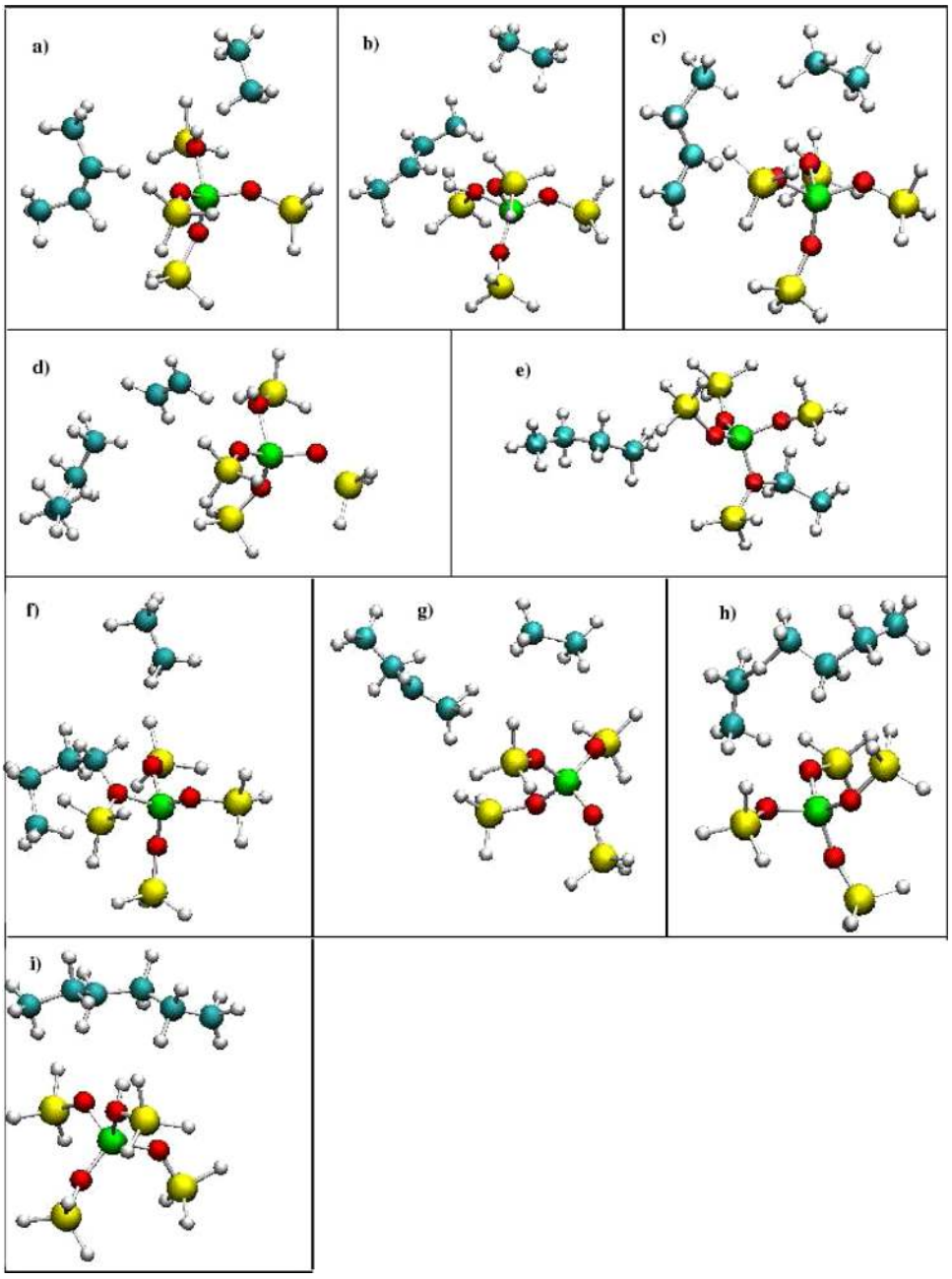

Figure 8. Structure calculations for C_6H_{14} C_2-C_3 on ZSM-5 after 1 ps: (a) C_2H_6 + *cis*-2-butene; (b) C_2H_6 + *trans*-2-butene; (c) C_2H_6 + 1-butene; (d) C_2H_4 + C_4H_{10}; (e) alkoxide for C_2H_5O + C_4H_{10}; (f) alkoxide for C_4H_9O + C_2 H_6; (g) C_2H_6 + C_4H_9; (h) trajectories which are still not cracked; (i) recrosing.

was in C−H−C intermediate state. After 4000 steps, this trajectory is forming an alkoxide structure, C_2H_5O, and C_4H_{10}. For forming the final products, for the C−H−C intermediate structure it is necessary to run more than 4000 steps. On the other hand, for the structures which after 2000 steps have formed alkoxides, which are relatively stable intermediates, 4000 steps are enough for reaching the final products.

Figure 10 displays the distances from the TS as a function of time for the C_2-C_3 cracking process.

For the Figure 10 the distance between the C_1-C_2 atoms in the TS position and the C_1-C_2 atoms in the product positions have been calculated as a function of time. The distance of C_1-C_2 from TS to the products have been calculated according to the equation

$$\sum_{i=1}^{2} \frac{R(C_i^{TS}(t=0) - C_i^{\text{Intermediate/Product}}(t))}{2} \tag{8}$$

or for the distance of C_3-C_6 from TS to the products have been calculated according to the equation

$$\sum_{i=3}^{6} \frac{R(C_i^{TS}(t=0) - C_i^{\text{Intermediate/Product}}(t))}{4} \tag{9}$$

where R is equal to

$$\sqrt{((x(i) - x(j))^2 + (y(i) - y(j))^2 + (z(i) - z(j))^2)}$$

and the results are shown by the black and the red lines in Figure 10. What we actually want to see is how the C_1-C_2 and

DOI: 10.1021/acs.jpcc.5b07457
J. Phys. Chem. C 2015, 119, 28836−28853

Table 4. QCT Product Distribution for C_6H_{14} C_2-C_3 Structure on ZSM-5

molecule	% products-673 K	% products-773 K	% products-813 K
$C_2H_6 + C_4H_9$	16%	28%	8%
C_2H_6 + 1-butene	4%	2%	14%
C_2H_6 + 2-butene	2%	2%	2%
$C_2H_4 + C_4H_{10}$	2%	4%	6%
$C_2H_5 + C_4H_{10}$		4%	2%
alkoxide ($C_2H_5O + C_4H_{10}$)	20%	16%	16%
alkoxide ($C_4H_9O + C_2H_6$)		4%	4%
recrossing	18%	12%	12%
C−H−C carbocation	38%	28%	34%

Table 5. QCT Product Distribution for C_6H_{14} C_3-C_4 Structure on ZSM-5

molecule	% products-673 K	% products-773 K	% products-813 K
$C_3H_8 + C_3H_6$	2%	2%	4%
C_3H_8 + ciclopropane	16%	16%	14%
$C_3H_8 + C_3H_7$	26%	20%	30%
alkoxide ($C_3H_7O + C_3H_8$)	12%	14%	10%
recrossing	26%	36%	30%
C−H−C carbocation	18%	12%	12%

C_3-C_6 moves from the TS until the products are formed. Similar calculations have been done also for the cracking between the C_2-C_3 atoms (dotted blue line Figure 10).

In the TS, the structure has 21 atoms C_6H_{15}, one hydrogen comes from the zeolite structure. The cracking process takes place in three steps:

(1) The C_2-C_3 atoms crack completely only after 400 fs (blue line Figure 10). The blue line in Figure 10 shows how the C_2-C_3 atoms evolve until the bond is breaking. The C−H−C intermediate state usually occurs up to maximum 400 fs. An almost constant blue line in Figure 10 from 0 to 400 fs can be observed, meaning that in this region the formation of C−H−C intermediate state takes place. After 400 fs, an increase of the distance between C_2 and C_3 atoms can be detected, indicating that this bond was broken, see Figure 10.

(2) After cracking the C_2H_6 product is formed (black line Figure 10). This occurs also at about 400 fs which is revealed by a steeper black line afterward.

(3) C_4H_9 has one proton more which is part of the zeolite framework. Between 400 and 500 fs C_4H_9 is still connected to the zeolite framework (flat red curve). Then a proton is transferred to the zeolite, and after about 750 fs the free C_4H_8 is formed, (see red line Figure 10).

A slow motion of C_4H_8 (3 Å from the TS) compared to C_2H_6 (6.5 Å from the TS) can be observed.

Similar calculations have been done also for the case when the cracking takes place between atoms C_3-C_4. In this case propane and propene are formed. Figure 11 shows the C_3-C_4 cracking process. Up to about 400 fs the C_3-C_4 distance is nearly constant (2−2.5 Å) . The two halves of the molecule move slowly away from the TS. After about 400 fs, C_3H_8 moves separately, while the C_3H_7 is still connected to the zeolite framework. The C_3H_6 molecule is formed after approximately 800 fs. Over this period of time C_3H_8 moves 4.5 Å away from the initial TS, while C_3H_6 diffuses 1.5 Å away from the initial TS. The dotted green line shows the movement of the alkoxide structure (the line is nearly horizontal). The alkoxide is stabilized near the zeolite acid site starting from 650 fs. The dotted blue line shows the motion of the C_3-C_4 atoms to be cracked. Similar as for Figure 10, also in Figure 11 the formation of the C−H−C intermediate is formed up to 400 fs. From 0 to 400 fs, a very small movement is observed in this region (C−H−C intermediate state), but the system is cracked after 400 fs. At about 800 fs the C_3H_8 movement levels out somewhat owing to the opposite zeolite wall.

C. Trajectories of C_6H_{14} on Y Zeolite. In this section, the QCT trajectories of C_6H_{14} on Y zeolite are discussed. For the C_1-C_2 cracking as final products only (a) CH_4 + *cis*-2-pentene have been obtained, and as intermediate states (b) $CH_4 + C_5H_{11}$ and (c) alkoxide for $CH_4 + C_5H_{11}$ O were found.

In Table 6 the cracking (C_2-C_3) structures on Y zeolite are shown. The final products obtained for this structure are (a) $C_2H_4 + C_4H_{10}$; (b) C_2H_6 + 1-butene; (c) C_2 H_6 + *trans*-2-butene. And the intermediates states formed are (a) $C_2H_6 + C_4H_9$; (b) $C_2H_5 + C_4H_{10}$; (c) alkoxide ($C_2H_5O + C_4H_{10}$); and (d) alkoxide ($C_4H_9O + C_2H_6$). Recrossings and carbocation trajectories have been also found. The increase of formation of final products (C_2H_6 + 1-butene is 2% at 773 K and 12% at 813 K) and the decrease of the formation of intermediate products ($C_2H_6 + C_4H_9$ goes from 26% at 773 K to 20% at 813 K, $C_2H_5 + C_4H_{10}$ goes from 10% at 773 K to 8% at 813 K and the alkoxide goes from 12% at 773 K to 10% at 813 K). Due to the increase of the number of final products and the decrease of the intermediate states, the number of trajectories which form the reactants are reduced from 36% at 773 K to 28% at 813 K. The TS for Y structure leads to the formation of a larger amount of product than the corresponding TS for ZSM-5. This might be due to the fact that the distance d(O···H) is smaller for Y structure (1.68 Å) than for ZSM-5 (1.79 Å). Now the details of the mechanism will be discussed.

In Figure 12, there are snapshots shown of how some products are formed starting from the TS C_2-C_3. The acidic hydrogen is shared by C_2-C_3 fragments for the first 336 fs. The C_2-C_3 bond length is enlarged. At about 336 fs a C_2-H-C_3 is formed. After 336 fs, the hydrogen can be transferred either to the C_2 or C_3 atoms. When it is transferred to atom C_3, C_4H_{10} is formed. This occurs at about 372 fs. This leaves the C_2 fragment as $C_2H_5^+$ which forms an alkoxide intermediate structure after 462 fs. At around 469 fs, C_2H_4 is formed. It should be noted that between 372 and 462 fs the $C_2H_5^+$ fragment is not connected to the zeolite framework. The second trajectory reveals similar sharing of the acidic H for more than 324 fs, but then the H is transferred to the C_2 structure forming C_2H_6 after 338 fs. This leaves the C_4 fragment $C_4H_9^+$ which can either deprotonate and forms C_4H_8 between 670 and 677 fs. In general, the alkoxide structures are formed after 624 fs. The third trajectory results also in a C_2-H-C_3 after 398 fs. Such a structure all three trajectories have in common. At 492 fs a C_4H_{10} molecule and a $C_2H_5^+$ ion are formed. At about 624 fs alkoxide is created which is even stable after 720 fs. As can be seen from the same TS various products can be generated. In all cases, first a C−H−C structure is formed. Then, depending on where the hydrogen atom goes, different fractions of alkanes and alkenes or alkoxides are created. The QCT automatically gives these

DOI: 10.1021/acs.jpcc.5b07457
J. Phys. Chem. C 2015, 119, 28836−28853

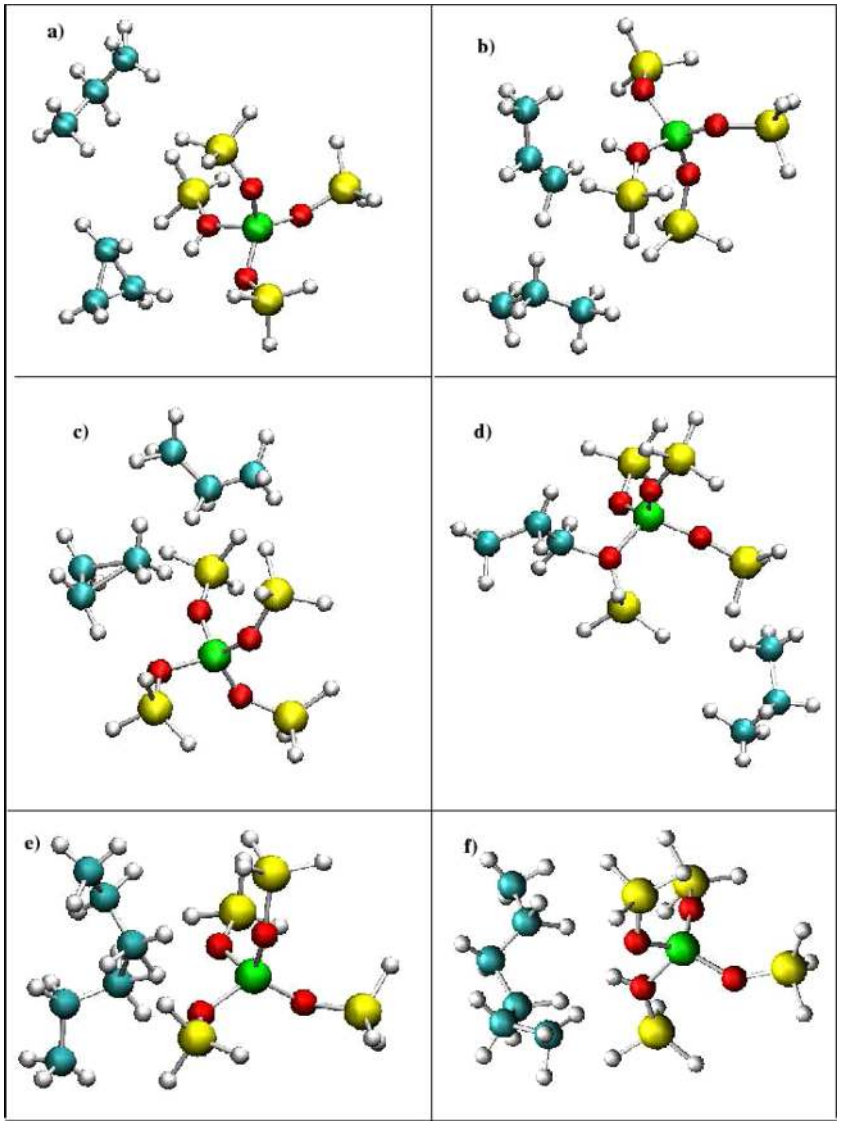

Figure 9. Structure calculations for C_6H_{14} C_3-C_4 on ZSM-5 after 1 ps: (a) C_3H_8 + cyclopropane ; (b) C_3H_8 + C_3H_6; (c) C_3H_8 + C_3H_7; (d) alkoxide; (e) trajectories which are still not cracked; (f) recrosing.

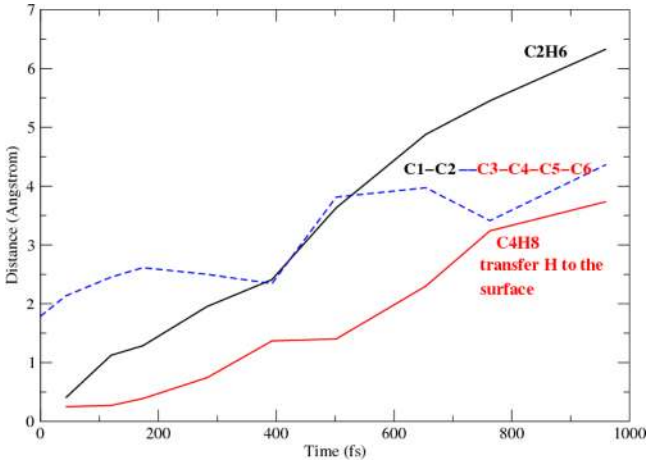

Figure 10. Distance from C_2-C_3 TS to final products for *n*-hexane cracking on ZSM-5.

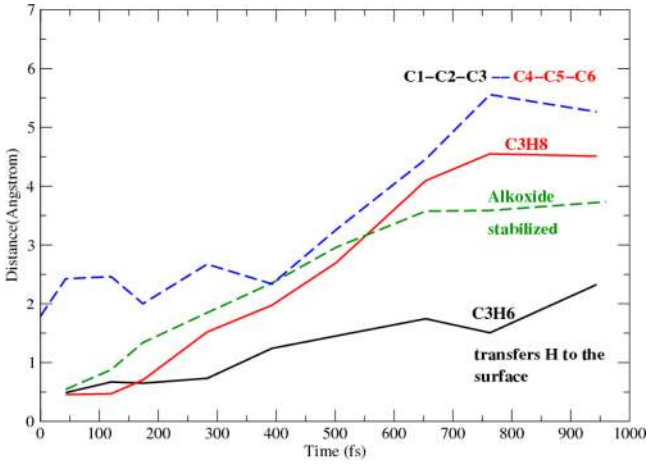

Figure 11. Distance from C_3-C_4 TS to final products for *n*-hexane cracking on ZSM-5.

final products. By calculating several trajectories, the statistics of the product distribution can be obtained. The mechanistic details have been found also in some previous papers.[16,26] The movement of the molecules as a function of time can, of course,

DOI: 10.1021/acs.jpcc.5b07457
J. Phys. Chem. C 2015, 119, 28836−28853

Table 6. QCT Product Distribution for C_6H_{14} C_2-C_3 Structure on Y

molecule	% products-673 K	% products-773 K	% products-813 K
$C_2H_4 + C_4H_{10}$	2%	8%	8%
C_2H_6 + 1-butene	6%	2%	12%
C_2H_6 + *trans*-2-butene	2%		
$C_2H_6 + C_4H_9$	12%	26%	20%
$C_2H_5 + C_4H_{10}$	16%	10%	8%
alkoxide (C_2H_5O + C_4H_{10}	8%	12%	10%
alkoxide (C_4H_9O + C_2H_6)	4%	6%	6%
recrossing	36%	28%	28%
C−H−C carbocation	14%	8%	8%

Table 7. QCT Product Distribution for C_6H_{14} C_3-C_4 Structure on Y

molecule	% products-673 K	% products-773 K	% products-813 K
$C_3H_8 + C_3H_6$	12%	12%	16%
C_3H_8 + ciclopropane	4%	4%	4%
$C_3H_8 + C_3H_7$	30%	24%	24%
alkoxide (C_3H_7O + C_3H_8)	4%	18%	6%
alkoxide (C_2H_4 + C_4H_9O)		2%	2%
recrossing	24%	22%	22%
C−H−C carbocation	26%	18%	26%

can only be found by QCT or other time-dependent methods.[90]

In Table 7 the (C_3-C_4) cracking structures on zeolite Y are shown. The final products obtained are propane and propene or propane and cyclopropane. Regarding the intermediate states, the only compounds observed are the alkoxide C_4H_9 O + C_2H_4. The temperature effect on C_3-C_4 cracking is very small. Only a slight increase of the products $C_3H_8 + C_3H_6$ from 12% to 16% and the decrease of the alkoxide $C_3H_7O + C_3H_8$ structure from 18% at 773 K to 6% at 813 K have been found.

In Figure 13, three different types of snapshots are shown: top - $C_3H_8 + C_3H_6$; middle - C_3H_8 + cyclopropane, and bottom - alkoxide formation. Looking at these three snapshots, one observes that the duration of the C−H−C intermediate varies from 42 to 314 fs. The first step starts from the TS C_3-C_4, Figure 13a. For the first trajectory, the acidic hydrogen is shared by C_3-C_4 fragments for the first 204 fs. After 204 fs hydrogen is transferred, and the C_3H_8 and the C_3 fragment as $C_3H_7^+$ are formed. $C_3H_7^+$ forms an alkoxide structure after 535 fs. The C_3H_6 is formed after 663 fs. In the second row cyclopropane is formed after 849 fs. The third row shows the formation of alkoxide after 488 fs and it is still there after 683 fs.

In the Tables 4-7 the product and intermediate distributions resulting from the three transition states are presented. Owing to the different energy barriers and other influences the compositions are different. If one assumes that the alkoxides, C_4H_9, C_3H_7, C_2H_5 and cyclopropane finally are converted into the products C_2H_6, 1,2-butene, C_4H_{10}, C_3H_6, C_3H_8, CH_4 and C_5H_{12} one could estimate the combined product distributions determined from QCTs starting from the three TSs.

V. DIFFERENCES BETWEEN *N*-HEXANE ON ZSM-5 AND Y

In this section the difference between *n*-hexane adsorbed and cracked on ZSM-5 and Y zeolites are discussed.

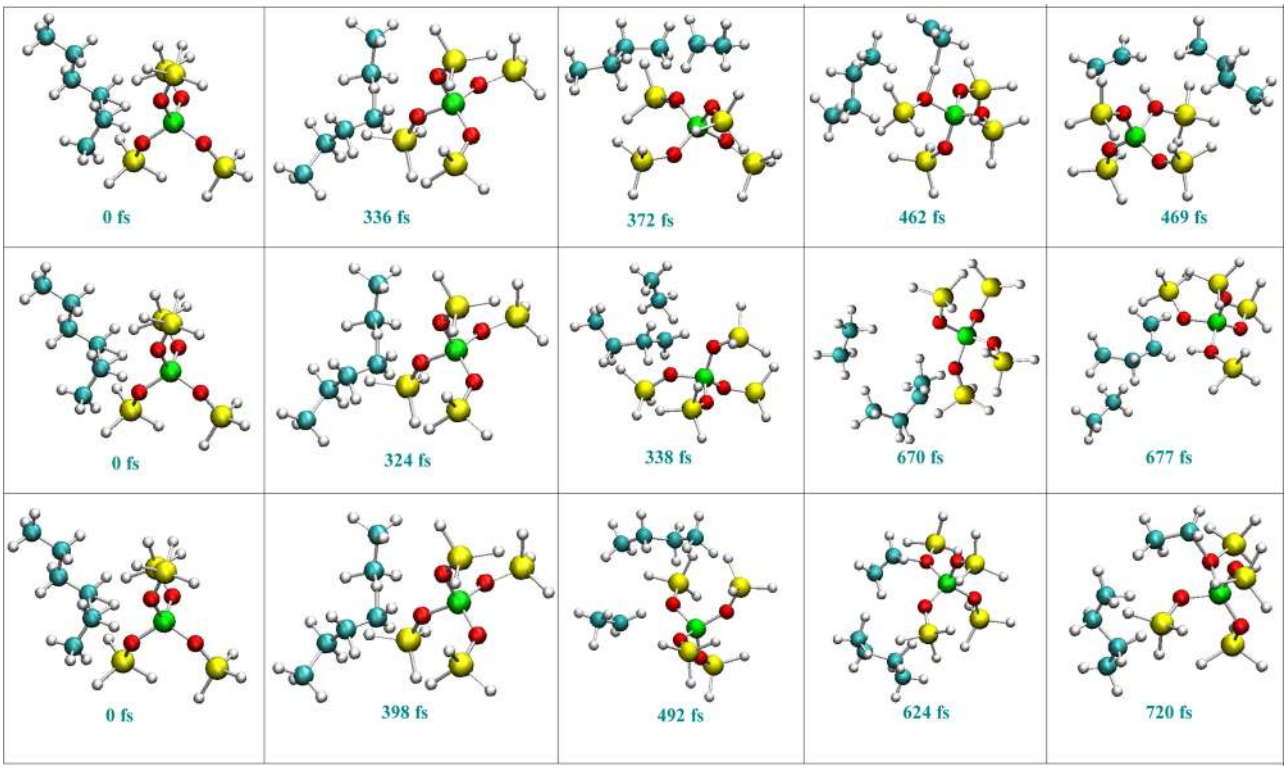

Figure 12. Snapshots of trajectories from TS 2−3 Y zeolite. Top $C_2H_4 + C_4H_{10}$, middle: $C_2H_6 + C_4H_8$, bottom: alkoxide formation.

DOI: 10.1021/acs.jpcc.5b07457
J. Phys. Chem. C 2015, 119, 28836−28853

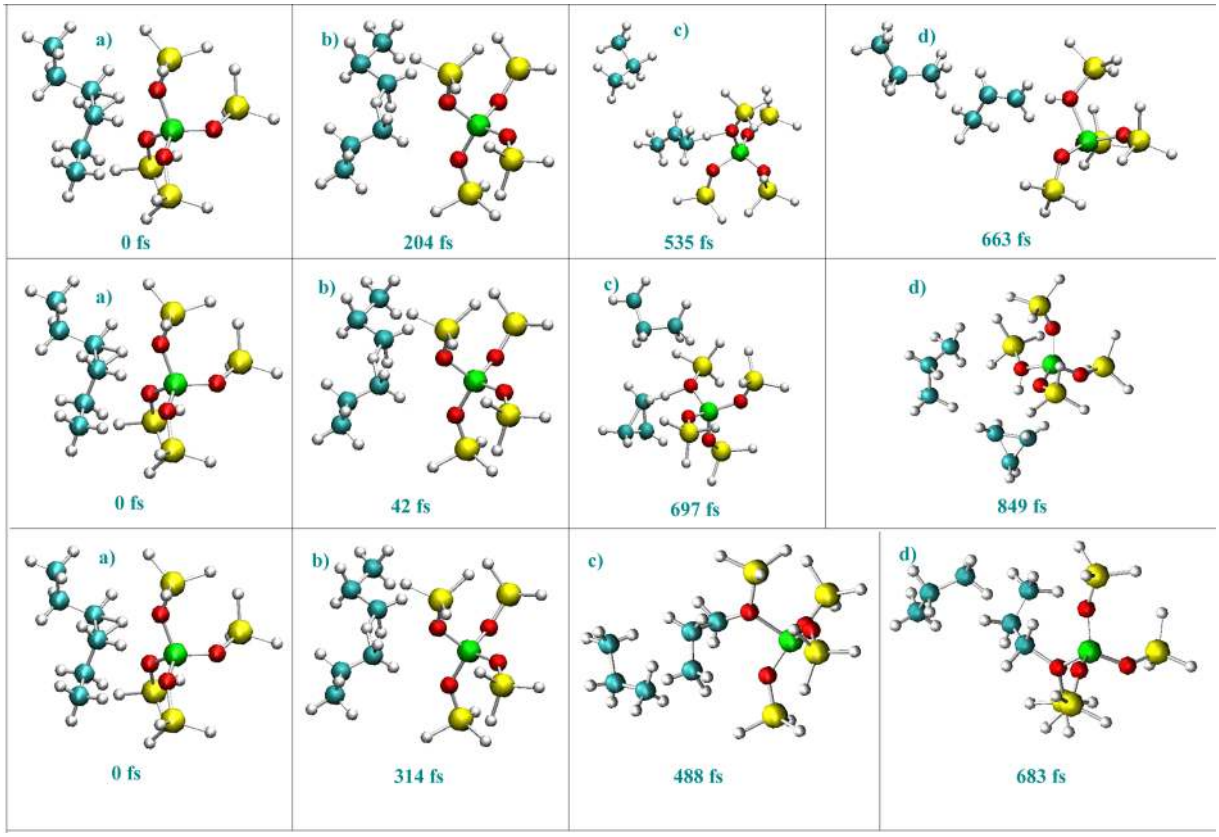

Figure 13. Snapshots of trajectories from TS 3−4 Y zeolite. Top: C_3H_8 + C_3H_6, middle: C_3H_8 + cyclopropane, bottom: alkoxide formation.

The faujasite framework consists of sodalite cages which are connected through hexagonal prisms. This creates the so-called supercage with four, tetrahedrally oriented, 12-ring pore openings and a 3-dimensional channel. The MFI class of zeolites has channels with diameters of ∼5.5 Å, whereas the faujasite zeolites (Y) have supercages with pores of ∼8 Å and internal diameters of ∼13 Å. The MFI zeolite structure contains a small concentration of aluminum in the framework. Thus, their cation exchange properties allow the introduction of acidic OH-groups via the well-known zeolite ion exchange reactions, which are essential factors for the development of acid hydrocarbon catalysis properties.

The thermodynamic properties investigated in this article have revealed the following differences between the MFI and Y zeolites:

- approximately 50 kJ/mol difference between the adsorption energy and adsorption enthalpy of *n*-hexane. The adsorption inside ZSM-5 is stronger owing to the narrower pores.
- the intrinsic activation energy differences are almost in the same range for both ZSM-5 and Y structures. The difference of 36 kJ/mol between the E_{act} of ZSM-5 and Y comes from the difference in adsorption energies.
- the theoretical intrinsic activation enthalpy data of ZSM-5 are in good agreement with the experimental values. The intrinsic activation enthalpies have been calculated for temperatures of 573 and 773 K. The intrinsic activation enthalpy for Y zeolite has been also calculated at these temperatures.
- the adsorption energy and the temperature play an important role for the calculations of the intrinsic activation enthalpy. Thus, the intrinsic activation enthalpy of *n*-hexane on Y is approximately 52 kJ/mol lower than the one obtained for ZSM-5. This is due to the differences in pore sizes.
- QCT trajectory calculations in the temperature range between 673 and 813 K show an influence in particular of the (C_2−C_3) product amounts of both for the ZSM-5 and Y zeolite. Increasing the temperature enhances generating more final products for (C_2−C_3) cracking. For the temperature range investigated, the (C_3−C_4) amount of products is only weakly influenced.

For the product distribution of C_6H_{14} C_2−C_3 structure one finds the following:

- For ZSM-5 zeolite at 673 and 773 K we have obtained 8% final products, namely C_2H_6 + 1-Butene/2-Butene and C_2 H_4 + C_4H_{10}. At 813 K an increase of the final products is observed from 8% to 22%. The concentration of the intermediate states decrease (C_4H_9, C_2H_5, C_3H_7, C_2H_5O, C_4H_9O, and C_3H_7O) with increasing temperature.
- For Y zeolite at 673 K - 8% products, at 773 K - 10% products, and at 813 K - 20% products were found.

The differences between ZSM-5 and Y zeolites for C_2−C_3 structure are

- For ZSM-5 the recrossing varies from 18% to 12%, while for Y zeolite it varies from 36% to 28% with increasing temperature from 673 to 813 K. These findings are given automatically by using QCT or other time-dependent approaches.[90] Variational transition state theory allows also to calculate transmision coefficients.

DOI: 10.1021/acs.jpcc.5b07457
J. Phys. Chem. C 2015, 119, 28836−28853

- For ZSM-5 the C−H−C carbocation intermediate structure is formed at an amount of 28−38%, and for Y zeolite the values are between 8% and 14% which corresponds to the larger amount of recrossing for Y zeolite.

From the differences mentioned above it is observed that ZSM-5 structure has approximately 38% C−H−C intermediate states, compared with about 14% of C−H−C intermediate states found for Y zeolite. These data lead to the conclusion that for Y zeolite we will get nearly 20% more reactants than for ZSM-5 from C−H−C intermediates.

For the product distribution of C_6H_{14} C_3−C_4 structure we have observed the following:

- The ZSM-5 zeolite at 673 K - 813 K resulted in 18% products of C_3H_8 + C_3H_6 and C_3H_8 + cyclopropane.
- The Y zeolite at 673 and 773 K gave 16% final products, and 20% final products at 813 K have been obtained.

The recrossing trajectories for ZSM-5 are between 26% and 36% and for Y zeolite the values are between 24% and 22%. The C−H−C intermediate structures found for ZSM-5 are between 18% and 12% and for Y zeolite 26%.

For the C_3−C_4 structures of ZSM-5 resulted in approximately 6% less C−H−C intermediates than the Y zeolite.

A. Product Distribution for ZSM-5 and Y Zeolites. Figure 14 shows a diagram of the products for the structures C_6H_{14}- on ZSM-5/Y zeolites compared with the experimental data.[8,9] The product distribution has been calculated for 773 K taking into account the final products and the intermediate states. The approach used is explained in detail in ref 86.

The final products obatained for the hexane cracking on ZSM-5 are

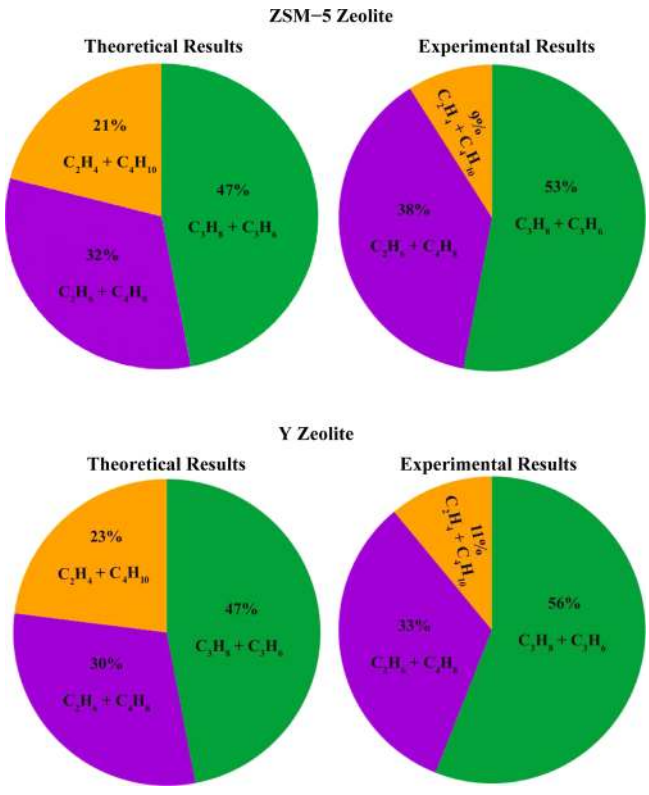

Figure 14. Diagram for the final products of hexane cracking on ZSM-5 and Y zeolites for T = 773 K.

- the most predominant product that has been obtained both theoretically and experimentally is C_3H_8 + C_3H_6. From the theoretical results C_3H_8 + C_3H_6 - 47%, and from the experiemntal results C_3H_8 + C_3H_6 - 53%
- C_2H_6 + C_4H_8 - 32% have been obtained from simulations and 38% from the experimental data[8,9,88]
- C_2H_4 + C_4H_{10} - 21% from the theoretical simulations and approximately 9% from the experimental data.[8,9,88]

The final products obatained for the hexane cracking on Y zeolite are

- C_3H_8 + C_3H_6 - 47% have been obtained from simulations and 56% from the experiments[8,9]
- C_2H_6 + C_4H_8 - 30% have been obtained from simulations and 33% from the experiments[8,9]
- C_2H_4 + C_4H_{10} - 23% have been obtained from simulations and 11% from the experiments[8,9]

VI. CONCLUSIONS

Adsorption thermodynamics and monomolecular cracking of *n*-hexane on ZSM-5 and Y zeolite have been studied by means of a QM/MM/QCT method. Thermodynamic properties presented in this article (such as adsorption energy, adsorption enthalpy, intrinsic activation energy, and intrinsic activation enthalpy) are influenced by the zeolite structure on which the adsorption and cracking occurs. The weaker adsorption energy obtained for Y zeolite influences also all other thermodynamic properties such as intrinsic activation energy or adsorption enthalpy etc.

Regarding the adsorption energy and/or intrinsic energy barrier data our calculated results are in qualitative and quantitative agreement with the experimental literature. From the thermodynamical properties calculations, the smaller activation barrier has been observed to be for C_6 H_{14} C_3−C_4. The dynamics simulations show the same trend as the thermodynamical properties calculations. Reaction dynamics plays a vital role in the cracking of *n*-hexane in H-MFI and Y zeolites. An important role plays the formation of the C−H−C intermediate state. This intermediate structure is formed imediately after the TS and influences the product formation. The procentage of C−H−C obtained within 1 ps is between 12% and 38%. This shows that these simulations can be ran more than 1 ps. Another important factor for obtaining the product distribution is played as expected by the temperature. Increasing the temperature leads to a decrease of the C−H−C intermediate state. Using information from these trajectories, an estimation of the product selectivity for *n*-hexane cracking have been obtained directly from simulations. Using the QCT method a variety of products have been obtained and compared to the experimental literature. The product distribution shows that the predominant product is C_3H_8 + C_3H_6 followed by C_2H_6 + C_4H_8 and C_2H_4 + C_4H_{10}. It has been shown that the QM/MM method chosen of a hybrid and dispersion corrected density functional by a relatively small computational effort.

AUTHOR INFORMATION

Notes

The authors declare no competing financial interest.

REFERENCES

(1) Corma, A. State of the Art and Future Challenges of Zeolites as Catalysts. *J. Catal.* **2003**, *216*, 298−312.
(2) Horsley, J. A. *CHEMTECH* **1997**, *27*, 45−49.

DOI: 10.1021/acs.jpcc.5b07457
J. Phys. Chem. C 2015, 119, 28836−28853

(3) Stoeker, M. Gas Phase Catalysis by Zeolites. *Microporous Mesoporous Mater.* **2005**, *82*, 257−292.
(4) Matsuda, T.; Kikuchi, E. Synthesis of Symmetrical Alkyl-Aromatics by use of Shape Selective Catalysts. *Res. Chem. Intermed.* **1993**, *19*, 319−332.
(5) Heinz, F. Selective Hydrocarbon Oxidation in Zeolites. *Science* **2006**, *313*, 309−310.
(6) Larsen, S. C. Applications of Zeolites in Environmental Catalysis. In *Environmental Catalysis*; Grassian, V. H., Ed.; CRC Press: Boca Raton, FL, 2005.
(7) Mignon, P.; Pidko, E. A.; Van Santen, R. A.; Geerlings, P.; Schoonheydt, R. A. Understanding the Reactivity and Basicity of Zeolites: A Periodic DFT Study of the Disproportionation of N2O4 on Alkali-Cation-Exchanged Zeolite Y. *Chem. - Eur. J.* **2008**, *14*, 5168−5177.
(8) Babitz, S. M.; Williams, B. A.; Miller, J. T.; Snurr, R. Q.; Haag, W. O.; Kung, H. H. Monomolecular Cracking of n-Hexane on Y, MOR, and ZSM-5 Zeolites. *Appl. Catal., A* **1999**, *179*, 71−86.
(9) Williams, B. A.; Ji, W.; Miller, J. T.; Snurr, R. Q.; Kung, H. H. Evidence of Different Reaction Mechanisms During the Cracking of n-Hexane on H-USY Zeolite. *Appl. Catal., A* **2000**, *203*, 179−190.
(10) Swisher, J. A.; Hansen, N.; Maesen, T.; Keil, F. J.; Smit, B.; Bell, A. T. Theoretical Simulation of n-Alkane Cracking on Zeolites. *J. Phys. Chem. C* **2010**, *114*, 10229−10239.
(11) Hansen, N.; Brüggemann, T.; Bell, A. T.; Keil, F. J. Theoretical Investigation of Benzene Alkylation with Ethene over H-ZSM-5. *J. Phys. Chem. C* **2008**, *112*, 15402−15411.
(12) Hansen, N.; Krishna, R.; van Baten, J. M.; Bell, A. T.; Keil, F. J. Analysis of Diffusion Limitation in the Alkylation of Benzene over H-ZSM-5 by Combining Quantum Chemical Calculations, Molecular Simulations, and a Continuum Approach. *J. Phys. Chem. C* **2009**, *113*, 235−246.
(13) Hansen, N.; Krishna, R.; van Baten, J. M.; Bell, A. T.; Keil, F. Reactor Simulation of Benzene Ethylation and Ethane Dehydrogenation Catalyzed by ZSM-5: A multiscale Approach. *Chem. Eng. Sci.* **2010**, *65*, 2472−2480.
(14) Bell, A. T.; Head-Gordon, M. Quantum Mechanical Modeling of Catalytic Processes. *Annu. Rev. Chem. Biomol. Eng.* **2011**, *2*, 453−477.
(15) Rigby, A. M.; Kramer, G. J.; van Santen, R. A. Mechanisms of Hydrocarbon Conversion in Zeolites: A Quantum Mechanical Study. *J. Catal.* **1997**, *170*, 1−10.
(16) Frash, M. V.; van Santen, R. A. Quantum-Chemical Modeling of the Hydrocarbon Transformations in Acid Zeolite Catalysts. *Top. Catal.* **1999**, *9*, 191−205.
(17) Hensen, E. J. M.; Pidko, E. A.; Rane, N.; van Santen, R. A. Modification of Brønsted Acidity of Zeolites by Ga^+, GaO^+ and AlO^+: Comparison for Alkane Activation. *Stud. Surf. Sci. Catal.* **2007**, *172*, 417−420.
(18) Pidko, E. A.; Santen, R. A. van. Activation of Light Alkanes over Zinc Species Stabilized in ZSM-5 Zeolite: A Comprehensive DFT Study. *J. Phys. Chem. C* **2007**, *111*, 2643−2655.
(19) Maginn, M. D.; Macedonia, E. J. Impact of Confinement in a Zeolite Cracking Selectivity via Monte Carlo Integration. *AIChE J.* **2000**, *46*, 2504−2517.
(20) Blaszkowski, S. R.; Jansen, A. P. J.; Nascimento, M. A. C.; van Santen, R. A. Density Functional Theory Calculations of the Transition States for Hydrogen Exchange and Dehydrogenation of Methane by a Brønsted Zeolite Proton. *J. Phys. Chem.* **1994**, *98*, 12938−12944.
(21) Kazansky, V. B.; Senchenya, I. N.; Frash, M.; van Santen, R. A. A Quantum-Chemical Study of Adsorbed Nonclassical Carbonium Ions as Active Intermediates in Catalytic Transformation of Paraffins. I. Protolytic Cracking of Ethane on High Silica Zeolites. *Catal. Lett.* **1994**, *27*, 345−354.
(22) Kazansky, V. B.; Frash, M.; van Santen, R. A. A Quantum-Chemical Study of Adsorbed Nonclassical Carbonium Ions as Active Intermediates in Catalytic Transformation of Paraffins. II. Protolyic Dehydrogenation and Hydrogen-Deuterium Hetero-Isotope Exchange of Paraffins on High-Silica Zeolites. *Catal. Lett.* **1994**, *28*, 211−222.
(23) Blaszkowski, S. R.; Nascimento, M. A. C.; van Santen, R. A. Activation of C-H and C-C Bonds by an Acidic Zeolite: A Density Functional Study. *J. Phys. Chem.* **1996**, *100*, 3463−3472.
(24) Zygmunt, S. A.; Curtiss, L. A.; Zapol, P.; Iton, L. E. Ab initio and Density Functional Study of the Activation Barrier for Ethane Cracking in Cluster Models of Zeolite H-ZSM-5. *J. Phys. Chem. B* **2000**, *104*, 1944−1949.
(25) Borges, P.; Ramos Pinto, R.; Lemos, M. A. N. D. A.; Lemos, F.; Vdrine, J. C.; Derouane, E. G.; Ram Ribeiro, F. Activity-Acidity Relationship for Alkane Cracking over Zeolites: n-Hexane Cracking over HZSM-5. *J. Mol. Catal. A: Chem.* **2005**, *229*, 127−135.
(26) Collins, S. J.; Omalley, P. J. A. Theoretical Description for the Monomolecular Cracking of C-C Bonds over Acidic Zeolites. *J. Catal.* **1995**, *153*, 94−99.
(27) Zheng, X.; Blowers, P. Reactivity of Alkanes on Zeolites: A Computational Study of Propane Conversion Reactions. *J. Phys. Chem. A* **2005**, *109*, 10734−10741.
(28) Haag, W. O. et al. *Proceedings of the 8th International Congress on Catalysis*; Verlag Chemie: Weinheim, 1994; Vol. *2*, p 35.
(29) Corma, A.; Planelles, J.; Snchez-Marn, J.; Toms, F. The Role of Different Types of Acid Site in the Cracking of Alkanes on Zeolite Catalysts. *J. Catal.* **1985**, *93*, 30−37.
(30) Thomas, C. L. Chemistry of Cracking Catalysts. *Ind. Eng. Chem.* **1949**, *41*, 2564−2573.
(31) Greensfelder, B. S.; Voge, H. H.; Good, G. M. Catalytic and Thermal Cracking of Pure Hvdrocarbons. *Ind. Eng. Chem.* **1949**, *41*, 2573−2584.
(32) Cumming, K. A.; Wojciechowski, B. W. Hydrogen Transfer, Coke Formation, and Catalyst Decay and Their Role in the Chain Mechanism of Catalytic Cracking. *Catal. Rev.: Sci. Eng.* **1996**, *38*, 101−157.
(33) Williams, B. A.; Babitza, S. M.; Millerb, J. T.; Snurra, R. Q.; Kung, H. H. The Roles of Acid Strength and Pore Diffusion in the Enhanced Cracking Activity of Steamed Y Zeolites. *Appl. Catal., A* **1999**, *177*, 161−175.
(34) Guzman, O.; Hernandez, F.; del Angel, P.; Velez, A. Cracking of N-Pentane over ZSM-5 Obtained from Different Seed Crystals. *React. Kinet. Catal. Lett.* **1994**, *52*, 475−480.
(35) Long-Xiang, T.; Lin-Sheng, W.; Mao-Song, X.; GuiFen, X.; Xue-Lin, W. New Method for Olefin Production from Light Alkanes. *React. Kinet. Catal. Lett.* **1994**, *53*, 205−209.
(36) Jentoft, F. C.; Gates, B. C. Solid-Acid-Catalyzed Alkane Cracking Mechanisms: Evidence from Reactions of Small Probe Molecules. *Top. Catal.* **1997**, *4*, 1−13.
(37) Corma, A.; Orchills, A. V. Current Views on the Mechanism of Catalytic Cracking. *Microporous Mesoporous Mater.* **2000**, *35*−*36*, 21−30.
(38) Kotrel, S.; Knoezinger, H.; Gates, B. C. The Haag-Dessau Mechanism of Protolytic Cracking of Alkanes. *Microporous Mesoporous Mater.* **2000**, *35*−*36*, 11−20.
(39) Kissin, V. V. Chemical Mechanisms of Catalytic Cracking over Solid Acid Catalysts: Alkanes and Alkenes. *Catal. Rev.: Sci. Eng.* **2001**, *43*, 85−146.
(40) Caeiro, G.; Carvalho, R. H.; Wang, X.; Lemos, M. A. N. D. A.; Lemos, F.; Guisnet, M.; Ribeiro, F. R. Activation of C_2-C_4 Alkanes over Acid and Bifunctional Zeolite Catalysts. *J. Mol. Catal. A: Chem.* **2006**, *255*, 131−158.
(41) Rahimi, N.; Karimzadeh, R. Catalytic Cracking of Hydrocarbons over Modified ZSM-5 Zeolites to Produce Light Olefins: A Review. *Appl. Catal. A: General* **2001**, *298*, 1−17.
(42) Derouane, E. G.; Vdrine, J. C.; Ramos Pinto, R.; Borges, P. M.; Costa, L.; Lemos, M. A. N. D. A.; Lemos, F.; Ram Ribeiro, F. The Acidity of Zeolites: Concepts, Measurements and Relation to Catalysis: A Review on Experimental and Theoretical Methods for the Study of Zeolite Acidity. *Catal. Rev.: Sci. Eng.* **2013**, *55*, 454−515.
(43) Cortright, R. D.; Dumesic, J. A.; Madon, R. J. Catalytic Cycles for Hydrocarbon Cracking on Zeolites. *Top. Catal.* **1997**, *4*, 15−26.

DOI: 10.1021/acs.jpcc.5b07457
J. Phys. Chem. C 2015, 119, 28836−28853

(44) Dellago, C.; Bolhuis, P. G. *Adv. Polym. Sci.* **2012**, 1−67.
(45) Bolhuis, P. G.; Chandler, D.; Dellago, C.; Geissler, P. L. Transition Path Sampling: Throwing Ropes over Mountain Passes in the Dark. *Annu. Rev. Phys. Chem.* **2002**, *53*, 291−318.
(46) Bucko, T.; Benco, L.; Hafner, J.; Angyan, J. G. Monomolecular Cracking of Propane over Acidic Chabazite: An ab initio Molecular Dynamics and Transition Path Sampling Study. *J. Catal.* **2011**, *279*, 220−228.
(47) Shao, Y.; et al. Advances in Methods and Algorithms in a Modern Quantum Chemistry Program Package. *Phys. Chem. Chem. Phys.* **2006**, *8*, 3172−3191.
(48) Olson, D. H.; Kokotailo, G. T.; Lawton, S. L.; Meier, W. M. Crystal Structure and Structure-Related Properties of ZSM-5. *J. Phys. Chem.* **1981**, *85*, 2238−2243.
(49) Olson, D. H.; Khosrovani, N.; Peters, A. W.; Toby, B. H. Crystal Structure of Dehydrated CsZSM-5 (5.8Al): Evidence for Nonrandom Aluminum Distribution. *J. Phys. Chem. B* **2000**, *104*, 4844−4848.
(50) Mentzen, B. F.; Sacerdote-Peronnet, M. Prediction of Preferred Proton Locations in HMFI/Benzene Complexes by Molecular Mechanics Calculations. Comparison with NMR, Structural and Calorimetric Results. *Mater. Res. Bull.* **1994**, *29*, 1341−1348.
(51) Zimmerman, P. M.; Tranca, D. C.; Gomes, J.; Lambrecht, D. S.; Head-Gordon, M.; Bell, A. T. Ab initio Simulations Reveal that Reaction Dynamics Strongly Affect Product Selectivity for the Cracking of Alkanes over H-MFI. *J. Am. Chem. Soc.* **2012**, *134*, 19468−19476.
(52) Field, M. J.; Bash, P. A.; Karplus, M. A Combined Quantum Mechanical and Molecular Mechanical Potential for Molecular Dynamics Simulations. *J. Comput. Chem.* **1990**, *11*, 700−733.
(53) Lyne, P. D.; Hodoscek, M.; Karplus, M. A Hybrid QM-MM Potential Employing Hartree-Fock or Density Functional Methods in the Quantum Region. *J. Phys. Chem. A* **1999**, *103*, 3462−3471.
(54) Woodcock, H. L.; Hododcek, M.; Gilbert, A. T. B.; Gill, P. M. W.; Schaefer, H. F.; Broks, B. R. Interfacing Q-Chem and CHARMM to Perform QM/MM Reaction Path Calculations. *J. Comput. Chem.* **2007**, *28*, 1485−1502.
(55) Zimmerman, P. M.; Head-Gordon, M.; Bell, A. T. Selection and Validation of Charge and Lennard-Jones Parameters for QM/MM Simulations of Hydrocarbon Interactions with Zeolites. *J. Chem. Theory Comput.* **2011**, *7*, 1695−1703.
(56) Lin, H.; Truhlar, D. G. QM/MM: what have we learned, where are we, and where do we go from here? *Theor. Chem. Acc.* **2007**, *117*, 185−199.
(57) Folope, N.; MacKerell, A. D. All-Atom Empirical Force Field for Nucleic Acids: I. Parameter Optimization based on Small Molecule and Condensed Phase Macromolecular Target Data. *J. Comput. Chem.* **2000**, *21*, 86−104.
(58) Grimme, S. Semiempirical GGA-Type Density Functional constructed with a Long-Range Dispersion Correction. *J. Comput. Chem.* **2006**, *27*, 1787−1799.
(59) Yamada, T.; Aida, M. Structures of Molecules in Ground and Excited Vibrational States from Quasiclassical Direct ab Initio Molecular Dynamics. *J. Phys. Chem. A* **2010**, *114*, 6273−6283.
(60) Ess, D. H.; Wheeler, S. E.; Iafe, R. G.; Xu, L.; Celebi-Olcum, N.; Houk, K. N. Bifurcations on Potential Energy Surfaces of Organic Reactions. *Angew. Chem., Int. Ed.* **2008**, *47*, 7592−7601.
(61) Baker, J. An Algorithm for the Location of Transition States. *J. Comput. Chem.* **1986**, *7*, 385−395.
(62) Lambrecht, D. S.; Clark, G. N. I.; Head-Gordon, T.; Head-Gordon, M. Simulated Photoelectron Spectra of the Cyanide-Water Anion via Quasiclassical Molecular Dynamics. *J. Phys. Chem. A* **2011**, *115*, 5928−5935.
(63) Porter, R.; Reff, L.; Miller, W. H. Quasiclassical Selection of Initial Coordinates and Momenta for a Rotating Morse Oscillator. *J. Chem. Phys.* **1975**, *63*, 2214−2218.
(64) Porter, R. Molecular Trajectory Calculations. *Annu. Rev. Phys. Chem.* **1974**, *25*, 317−355.
(65) Karplus, M.; Porter, R. N.; Sharma, R. D. Exchange Reactions with Activation Energy. I. Simple Barrier Potential for (H, H_2. *J. Chem. Phys.* **1965**, *43*, 3259−3287.
(66) Czako, G.; Kalendin, A. L.; Bowman, J. M. A Practical Method to Avoid Zero-Point Leak in Molecular Dynamics Calculations: Application to the Water Dimer. *J. Chem. Phys.* **2010**, *132*, 164103 (6 pag.).
(67) Cramer, C. J. *Essentials of Computational Chemistry*; John Wiley and Sons Ltd.: England, 2002; Chapter 10.
(68) Moor, B. A.; Reyniers, M. F.; Marin, G. B. Physisorption and Chemisorption of Alkanes and Alkenes in H-FAU: a Combined ab Initio-Statistical Thermodynamics Study. *Phys. Chem. Chem. Phys.* **2009**, *11*, 2939−2958.
(69) Moor, B. A.; Reyniers, M. F.; Gobin, O. C.; Lercher, J. A.; Marin, G. B. Adsorption of C2-C8 n-Alkanes in Zeolites. *J. Phys. Chem. C* **2011**, *115*, 1204−1219.
(70) Moor, B. A.; Ghysels, A.; Reyniers, M. F.; Van Speybroeck, V.; Waroquier, M.; Marin, G. B. Normal Mode Analysis in Zeolites: Toward an Efficient Calculation of Adsorption Entropies. *J. Chem. Theory Comput.* **2011**, *7*, 1090−1101.
(71) Evans, M. G.; Polanyi, M. Some Applications of the Transition State Method to the Calculation of Reaction Velocities, especially in Solution. *Trans. Faraday Soc.* **1935**, *31*, 875−894.
(72) Eyring, H. The Activated Complex in Chemical Reactions. *J. Chem. Phys.* **1935**, *3*, 107−115.
(73) McQuarrie, D. A. *Statical Mechanics*, 1st ed.; Harper Collins: New York, 1973.
(74) Ramachandran, C. E. Observation of a Compensation Relation for n-Hexane Adsorption in Zeolites with Different Structures: Implications for Catalytic Activity. *J. Catal.* **2005**, *233*, 100−108.
(75) Maihom, T.; Pantu, P.; Tachakritikul, C.; Probst, M.; Limtrakul, J. Effect of the Zeolite Nanocavity on the Reaction Mechanism of n-Hexane Cracking: A Density Functional Theory Study. *J. Phys. Chem. C* **2010**, *114*, 7850−7856.
(76) Xu, B.; Sievers, C.; Hong, S. B.; Prins, R.; van Bokhoven, J. A. Catalytic activity of Brnsted Acid Sites in Zeolites: Intrinsic Activity, Rate-Limiting Step, and Influence of the Local Structure of the Acid Sites. *J. Catal.* **2006**, *244*, 163−168.
(77) Narbeshuber, T. F.; Vinek, H.; Lercher, J. A. Monomolecular Conversion of Light Alkanes over H-ZSM-5. *J. Catal.* **1995**, *157*, 388−395.
(78) Abouelnasr, M. K. F.; Smit, B. Diffusion in Confinement: Kinetic Simulations of Self- and Collective Diffusion Behavior of Adsorbed Gases. *Phys. Chem. Chem. Phys.* **2012**, *14*, 11600−11609.
(79) Gomes, J.; Zimmerman, P. M.; Head-Gordon, M.; Bell, A. T. Accurate Prediction of Hydrocarbon Interactions with Zeolites Utilizing Improved Exchange-Correlation Functionals and QM/MM Methods: Benchmark Calculations of Adsorption Enthalpies and Application to Ethene Methylation by Methanol. *J. Phys. Chem. C* **2012**, *116*, 15406−15414.
(80) Heyden, A.; Hansen, N.; Bell, A. T.; Keil, F. J. Nitrous Oxide Decomposition over Fe-ZSM-5 in the Presence of Nitric Oxide: A Comprehensive DFT Study. *J. Phys. Chem. B* **2006**, *110*, 17096−17114.
(81) Chai, J. D.; Head-Gordon, M. Long-Range corrected Hybrid Density Functionals with damped Atom-Atom Dispersion Corrections. *Phys. Chem. Chem. Phys.* **2008**, *10*, 6615−6620.
(82) Chai, J. D.; Head-Gordon, M. Systematic Optimization of Long-Range corrected Hybrid Density Functionals. *J. Chem. Phys.* **2008**, *128*, 084106 (15 pag.).
(83) Peslherbe, G. H.; Wang, H.; Wang, W. L. Monte Carlo Sampling for Classical Trajectory Simulations. *Adv. Chem. Phys.* **1999**, *105*, 171−201.
(84) Tranca, D. C.; Hansen, N.; Swisher, J. A.; Smit, B.; Keil, F. J. Combined Density Functional Theory and Monte Carlo Analysis of Monomolecular Cracking of Light Alkanes Over H-ZSM-5. *J. Phys. Chem. C* **2012**, *116*, 23408−23417.
(85) Zimmerman, P. M.; Tranca, D. C.; Gomes, J.; Lambrecht, D. S.; Head-Gordon, M.; Bell, A. T. Ab Initio Simulations Reveal that

DOI: 10.1021/acs.jpcc.5b07457
J. Phys. Chem. C 2015, 119, 28836−28853

Reaction Dynamics Strongly Affect Product Selectivity for the Cracking of Alkanes over H-MFI. *J. Am. Chem. Soc.* **2012**, *134*, 19468−19476.
(86) Tranca, D. C.; Keil, F. J. First-Principles Investigation of the Adsorption of the 2,5-Pyridine Di-Carboxylic Acid onto the Cu(011) Surface. *J. Chem. Phys.* **2011**, *134*, 104708 (15 pag.).
(87) von Bokhoven, J. A.; Williams, B. A.; Ji, W.; Koningsberger, D. C.; Kung, H. H.; Miller, J. T. Observation of a Compensation Relation for Monomolecular Alkane Cracking by Zeolites: the Dominant Role of Reactant Sorption. *J. Catal.* **2004**, *224*, 50−59.
(88) Narbeshuber, T. F.; Vinek, H.; Lercher, J. A. Monomolecular Conversion of Light Alkanes over H-ZSM-5. *J. Catal.* **1995**, *157*, 388−395.
(89) Sharada, S. M.; Zimmerman, P. M.; Bell, A. T.; Head-Gordon, M. Insights into the Kinetics of Cracking and Dehydrogenation Reactions of Light Alkanes in H-MFI. J. *J. Phys. Chem. C* **2013**, *117*, 12600−12611.
(90) Marx, D.; Hutter, J. *Ab initio Molecular Dynamics - Basic Theory and Advanced Methods*; Cambridge University Press: Cambridge, U.K., 2009.

DOI: 10.1021/acs.jpcc.5b07457
J. Phys. Chem. C 2015, 119, 28836−28853